Title

High Temporal Resolution Modeling of the Impact of Rain, Tides, and Sea Level Rise on Water Table Flooding in the Arch Creek Basin, Miami-Dade County Florida USA

Author Names and Affiliations

Michael C. Sukop[a]
Martina Rogers[b]
Greg Gaunnel[c]
Johnna M. Infanti[d,e]
Katherine Hagemann[f]

[a]Florida International University, Department of Earth and Environment, AHC-5 360, 11200 SW 8th Street, MIAMI, FL 33199 USA; email: sukopm@fiu.edu

[b]Broward College, 111 East Las Olas Boulevard, Fort Lauderdale, FL 33301 USA; email: rogem6@mail.broward.edu

[c]The University of the West Indies, St. Thomas Campus, 2 John Brewers Bay, St. Thomas, V.I. 00802-6004, USA; email: greg.guannel@gmail.com

[d]Rosenstiel School of Marine and Atmospheric Science, University of Miami, 4600 Rickenbacker Causeway, Miami, FL, 33149, USA; email: jinfanti@rsmas.miami.edu

[e]Florida Atlantic University, Center for Environmental Studies, 3200 College Ave., Davie, FL 33314, USA

[f]Office of Resilience, Miami-Dade County, 111 NW 1st Street, 12th Floor, Miami, Florida 33128, USA; email: Katherine.Hagemann@miamidade.gov

Corresponding author with contact details: E-mail address and full postal address

Michael C. Sukop, sukopm@fiu.edu

Florida International University
Department of Earth and Environment, AHC-5, 360
11200 SW 8th Street
MIAMI, FL 33199

Keywords

Groundwater, Sea Level Rise, Tides, Sunny-day flooding, Coastal flooding, Repetitive loss flooding

Abstract

Modeling of groundwater levels in a portion of the low-lying coastal Arch Creek basin in northern Miami-Dade County in Southeast Florida USA, which is subject to repetitive flooding, reveals that rain-induced short-term water table rises can be viewed as a primary driver of flooding events under current conditions. Areas below 0.9 m North American Vertical Datum (NAVD) elevation are particularly vulnerable and areas below 1.5 m NAVD are vulnerable to exceptionally large rainfall events. Long-term water table rise is evident in the groundwater data, and the rate appears to be consistent with local rates of sea level rise. Linear extrapolation of long-term observed groundwater levels to 2060 suggest roughly a doubling of the number of days when groundwater levels exceed 0.9 m NAVD and a threefold increase in the number of days when levels exceed 1.5 m NAVD. Projected sea level rise of 0.61 m by 2060 together with increased rainfall lead to a model prediction of frequent groundwater-related flooding in areas less than 0.9 m NAVD. However, current simulations do not consider the range of rainfall events that have led to water table elevations greater than 1.5 m NAVD and widespread flooding of the area in the past. Tidal fluctuations in the water table are predicted to be more pronounced within 600 m of a tidally influenced water control structure that is hydrodynamically connected to Biscayne Bay. The inland influence of tidal fluctuations appears to increase with increased sea level, but the principal driver of high groundwater levels under the 2060 scenario conditions remains groundwater recharge due to rainfall events.

1 Introduction

Low-lying coastal regions are vulnerable to increased flooding due to higher water tables brought on by high tides and sea level rise. Higher water tables reduce the potential subsurface storage of stormwater and the water table can rise above the land surface leading to flooding. Tidally-driven “sunny-day” or “nuisance” flooding phenomena are increasingly affecting numerous areas, including for example, Southeast Florida and Norfolk, Virginia (Corum, 2016). Wdowinski et al. (2016) recognized three types of flooding events (rain, tide, and storm surge) and detected significant increases in tidal and rain-based flooding in Miami Beach, Florida between 2006 and 2013. They noted that higher sea levels also increased the frequency of rain-induced flooding events and attributed the increase to reduced effectiveness of gravity-based drainage systems but did not consider water table changes. Pumps installed by the City of Miami Beach resulted in fewer flooding events.

Only a small number of scientific papers appear to address flooding due to groundwater inundation/emergence. Habel et al. (2017) use a steady state numerical model and Rotzoll and Fletcher (2013) used 1-dimensional steady state analytical solutions to investigate groundwater inundation in Hawaii, while Hoover et al. (2016) simply added sea level rise to existing groundwater levels to assess potential groundwater emergence on the California coast. The economic costs of flooding are substantial. Czajkowski, et al. (2018, this issue) provide a detailed analysis of flooding costs in the Miami area.

The data analysis and modeling efforts described here are motivated by a desire to better elucidate the mechanisms responsible for flooding in low-lying coastal environments and to provide physically-based models for projection of future flooding under conditions of higher sea levels and potentially higher rainfall amounts. Our goals are to assess the relative importance of tides and rainfall, and to begin to address questions such as the importance of surface permeability, which is often assumed to be the controlling factor in flooding. Storm-related flooding is often regarded as a surface water drainage problem that is addressed with different analytical tools, but the intimate coupling of surface and groundwater in some regions may permit the flooding problem to be usefully viewed primarily as a groundwater problem. The groundwater aspect of flooding may be of paramount importance in areas that rely on on-site septic systems.

1.1 Study Area

This study considers a portion of the 11.5 km^2 Arch Creek Basin (part of the North Biscayne Bay watershed) in northernmost Miami-Dade County in Southeast Florida USA (Figures 1 and 2) and it focuses on the low-lying Arch Creek Estates subdivision portion of the basin (Figure 2), which was platted in the 1940s (Miami-Dade, 2016) and built in an area recognized as especially low lying and not recommended for development (U.S. Army Corps of Engineers, 1958). Thirty-four repetitive loss properties and three severe repetitive loss properties are located in this area, which was Focus Area 3 of an Urban Land Institute study in 2016 (ULI, 2016).

The full Arch Creek basin includes land belonging to five jurisdictions: North Miami (7.2 km^2), Miami Shores (0.2 km^2), Biscayne Park (1.3 km^2), and North Miami Beach (0.4 km^2) with the remaining 2.3 km^2 being part of unincorporated Miami-Dade County.

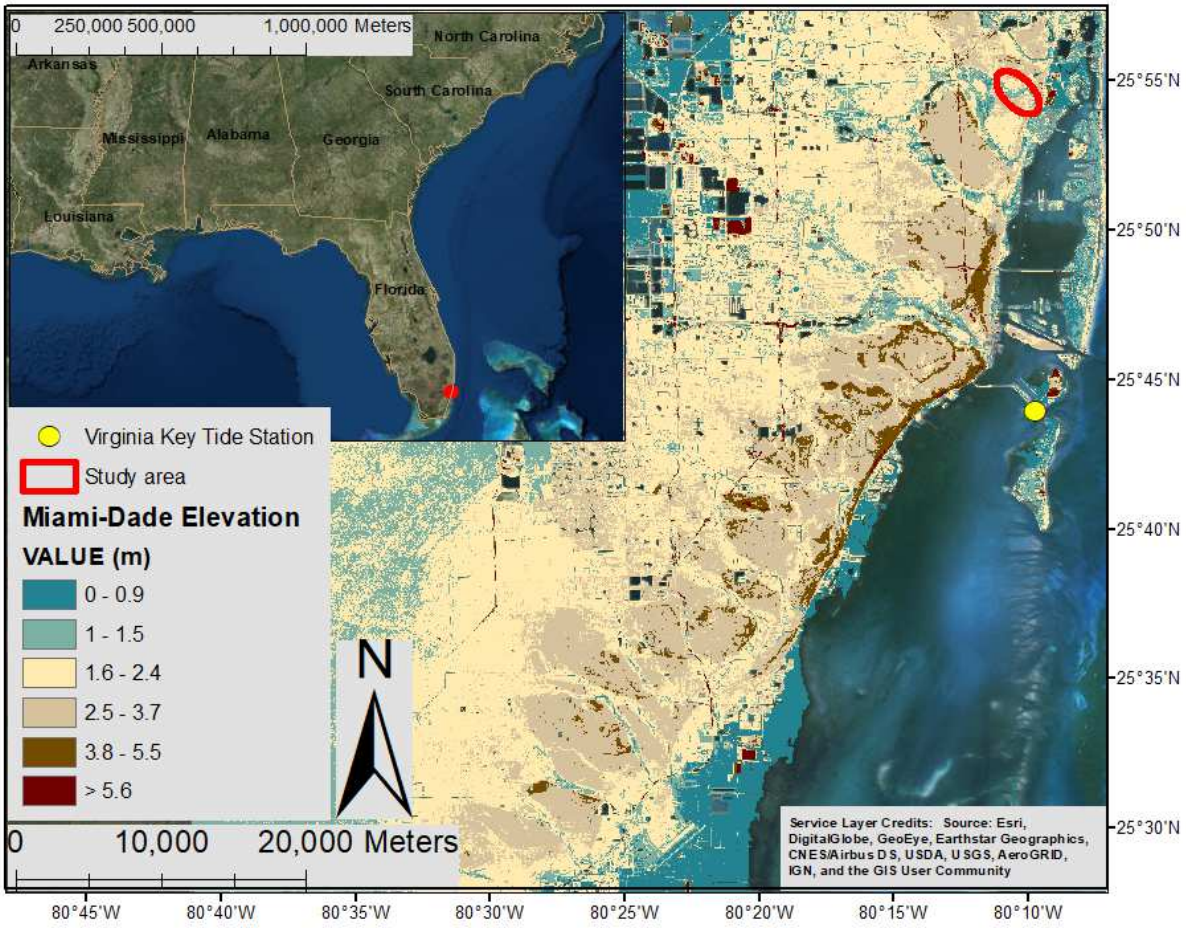

Figure 1. Location of study area and Virginia Key tide station. LiDaR topography shows Atlantic Coastal Ridge and transverse glades. Elevations in meters relative to the North American Vertical Datum of 1988 (NAVD 88).

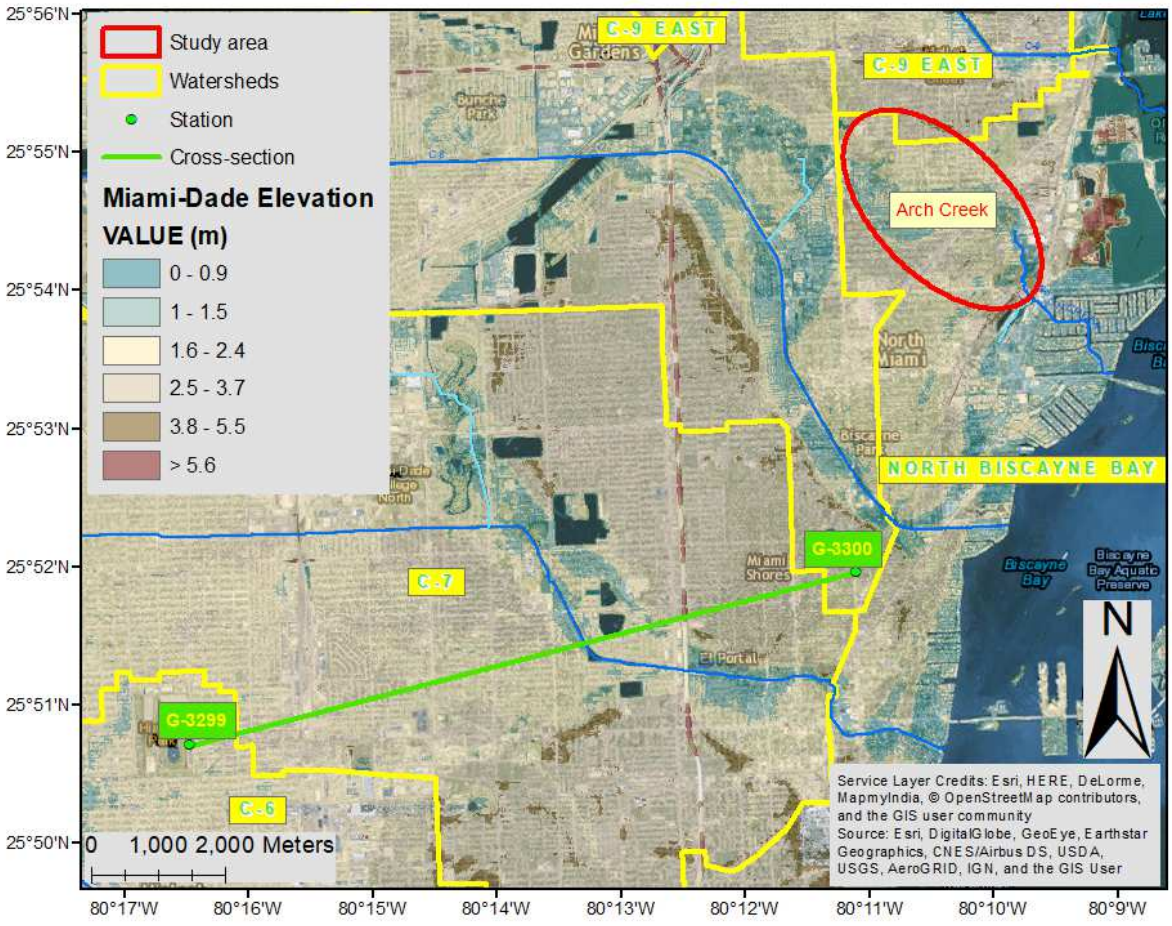

Figure 2. Watersheds (yellow) including North Biscayne Bay watershed that encloses Arch Creek study area (red ellipse), with LiDaR topography, location of Spur Canal No. 4 west of study area (light blue), and location of nearest geologic cross-section (green) from study of Fish and Stewart (1991).

Miami-Dade County has prioritized mitigation activities in repetitive loss areas (M-D, 2017). Florida passed legislation in 2013 (163.3177 f.s.) creating an Adaptation Action Area designation where local governments "...may consider policies within the coastal management element to improve resilience to coastal flooding resulting from high-tide events, storm surge, flash floods, stormwater runoff, and related impacts of sea-level rise." Miami-Dade County included Adaptation Action Areas in its Comprehensive Development Master Plan in 2015. The Arch Creek Basin is Miami-Dade County's pilot Adaptation Action Area (M-D, 2017).

1.2 Topography

South Florida has low relief, but subtle differences in elevation on the order of a few meters are readily discernable from LiDaR data (Figures 1 and 2). The Digital Elevation Model used throughout this paper is a 2m spatial resolution product (UTM 17N Horizontal Datum WGS84 and Vertical Datum NAVD 1988). The Atlantic Coastal Ridge is a northeast-trending ridge parallel to the coast. The ridge is cut by a series of southeast-trending 'transverse glades' that

were natural outlets for flow from the Everglades west of the ridge and which have often been exploited for the dredging of canals to enhance Everglades and local drainage.

The LiDaR data and aerial photography (Figure 2) show the ancestral floodplains and the extensive development that has occurred in them.

1.3 Repetitive Loss Properties

A number of residential properties in the Arch Creek basin have been subject to repetitive losses due to flooding. Figure 3 shows the approximate locations of the properties in the context of the topography.

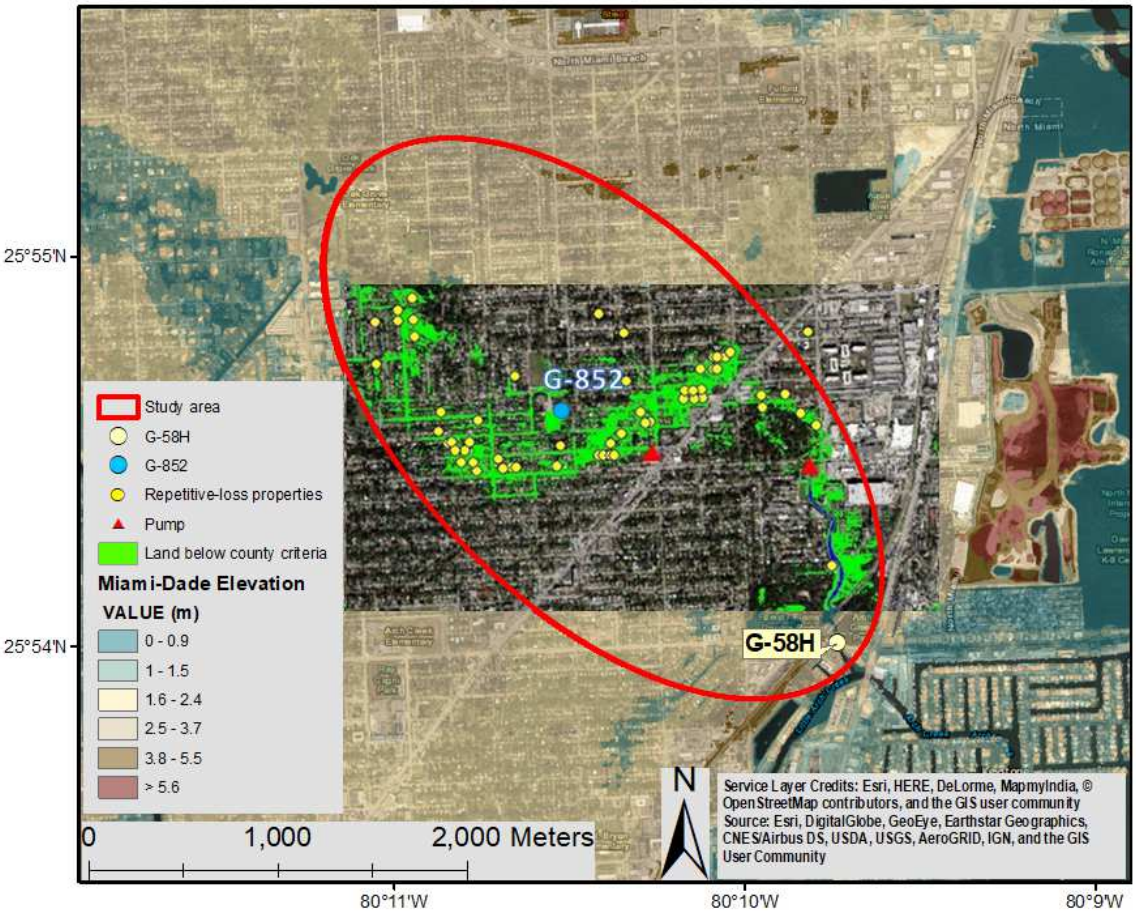

Figure 3. Sites of repetitive-loss properties in study area (yellow dots), locations of pumps (red triangles), observation well G-852 (blue dot), water control structure G-58 (white dot), and land below county flood criteria (green). Derived from ULI (2016).

1.4 Hydrology and Subsurface Hydrogeology

The South Florida region has a dry season in November through April, and a wet season in May through October. The 30-year (1986-2015) annual rainfall in Miami-Dade County is 1.47 m. Wet season rainfall comes primarily in the form of fast-moving, localized, and intense thunderstorms. The largest rainfall events are associated with tropical storms and hurricanes, which can also result in higher sea levels due to storm surge. Groundwater is generally within just a few meters of the surface. During pre-development times, water moved across the study area from the Everglades eastward through an extensive system of transverse glades (Figures 1 and 2) to Biscayne Bay. Currently, the hydrologic system is intensively managed with a large number of canals, salinity control structures, and pumps.

This management has multiple conflicting objectives that present challenges. The most important objective may be flood control, which aims to move water out to the sea quickly and to adjust groundwater levels to better accommodate impending storms. Second, the extensive network of salinity control structures is intended to maintain higher inland water levels in the canals and the groundwater system to prevent saltwater intrusion via the subsurface or via movement up the canals. Finally, the canal network, which also transports water from as far away as Orlando, Florida, serves to provide aquifer recharge that enables large-scale water extraction.

There are two pumps in the Arch Creek Estates study area that lift water either into a retention basin for water quality mitigation eventual discharge to the upper reaches of the current remaining part of the creek or for discharge into the underlying brackish water aquifer via 60 m deep drainage wells. There is a salinity control structure (G-58, Figure 3) that spans a low ridge near where Arch Creek meets the tidal channels connected to Biscayne Bay. This and numerous structures like it in coastal Southeast Florida are intended to maintain higher groundwater levels on the upstream side to limit subsurface saltwater intrusion and to limit upstream migration of saltwater in the canals during high tides and storms.

The Biscayne Aquifer is an eastward-thickening agglomeration of mostly limestone rock with some sand bodies and is the principal source of municipal, private, and agricultural irrigation water in Southeast Florida. The compilation of Fish and Stewart (1991) included cross-sections of subsurface Miami-Dade County. The nearest cross-section is about 4800 m south of the study area (Figure 2) and the eastern portion of their section A-A’ is reproduced in Figure 4.

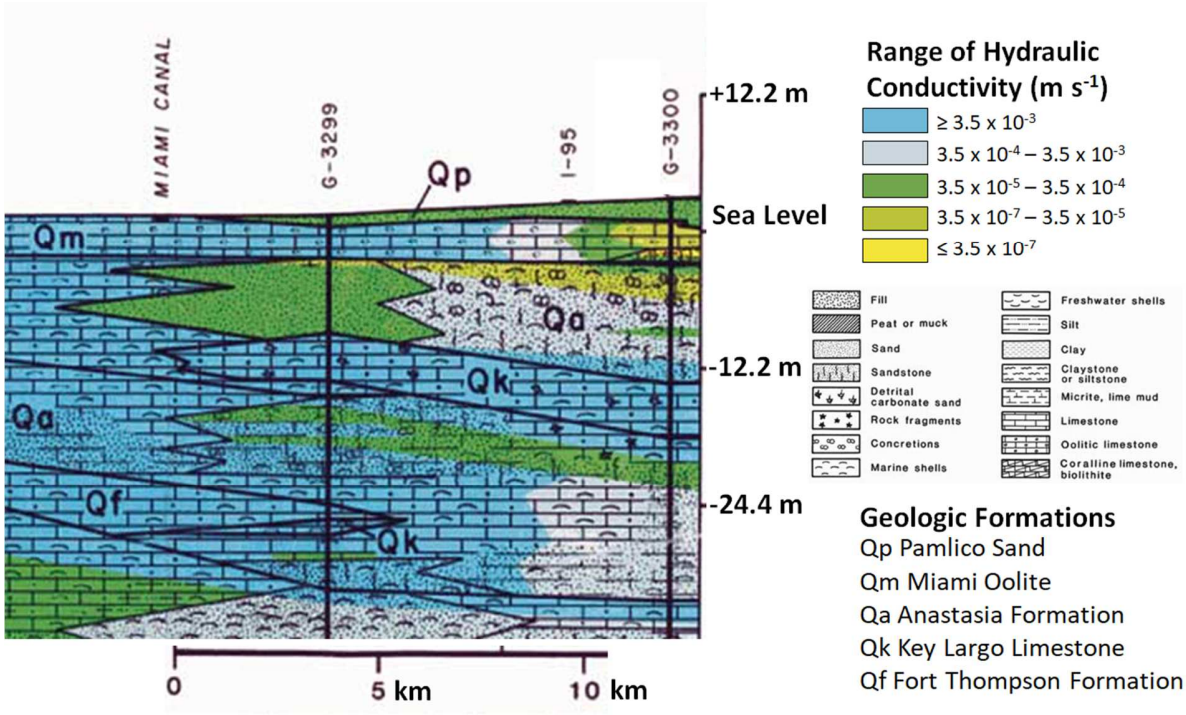

Figure 4. Geologic cross-section 5 km south of study area. Section location shown on Figure 2. Modified from Fish and Stewart (1991).

At USGS well G-3300 on the eastern end of the cross-section, which is expected to be most relevant to the study area, there are about 3 m of the Pamlico Sand formation overlying about 6 m of uncharacteristically low permeability Miami Oolite and 3 m of Anastasia Formation both with hydraulic conductivity less than 3.5 x 10^{-7} m s^{-1}. This was followed by 6 m of 3.5 x 10^{-4} m s^{-1} to 3.5 x 10^{-3} m s^{-1} hydraulic conductivity Anastasia Formation. The most permeable unit was the underlying 9 m of the Key Largo Limestone (greater than 3.5 x 10^{-3} m s^{-1}, suggesting a minimum transmissivity of 0.03 m^2s^{-1}). The transmissivity of the Biscayne Aquifer is much higher in some areas (Renken et al., 2005), due to the presence of zones of very high porosity with 2 cm pores (Sukop and Cunningham, 2014).

2 Methods

2.1 Analysis of Water Level Data

Following the Urban Land Institute workshop, a “Resilient Redesign” charrette dedicated to identifying potential adaptation to repetitive flooding and sea level rise in the Arch Creek basin was convened by the South Florida Regional Climate Change Compact and held in November 2016. As part of the workshop, a detailed analysis of readily available surface and groundwater data was undertaken.

The United States Geological Survey (USGS) provides statistical groundwater level compilations for South Florida. Figure 5 shows that the 75th-percentile end-of-wet-season groundwater levels in the study area are between 0 and a bit more than 0.3 m NAVD (Prinos and Dixon, 2016). The statistical analysis and spatial resolution of groundwater levels in these results may be adequate for understanding of some potential redesign options for the area, but provide no information on causality of high groundwater levels beyond the correlation with the wet season and are consequently less useful for assessing future groundwater levels under different conditions.

The USGS map may also be helpful for deciding on the potential appropriateness of various boundary conditions for groundwater models. In particular, Figure 5 shows a mound beneath the study area suggesting that flow may occur in the inland direction away from the sea during the wet season. This is consistent with the presence of Spur Canal No. 4 which runs northeast off of the C-8 canal (Figure 2) and provides drainage to the northwestern edge of the study area. Model boundary conditions are discussed in additional detail below.

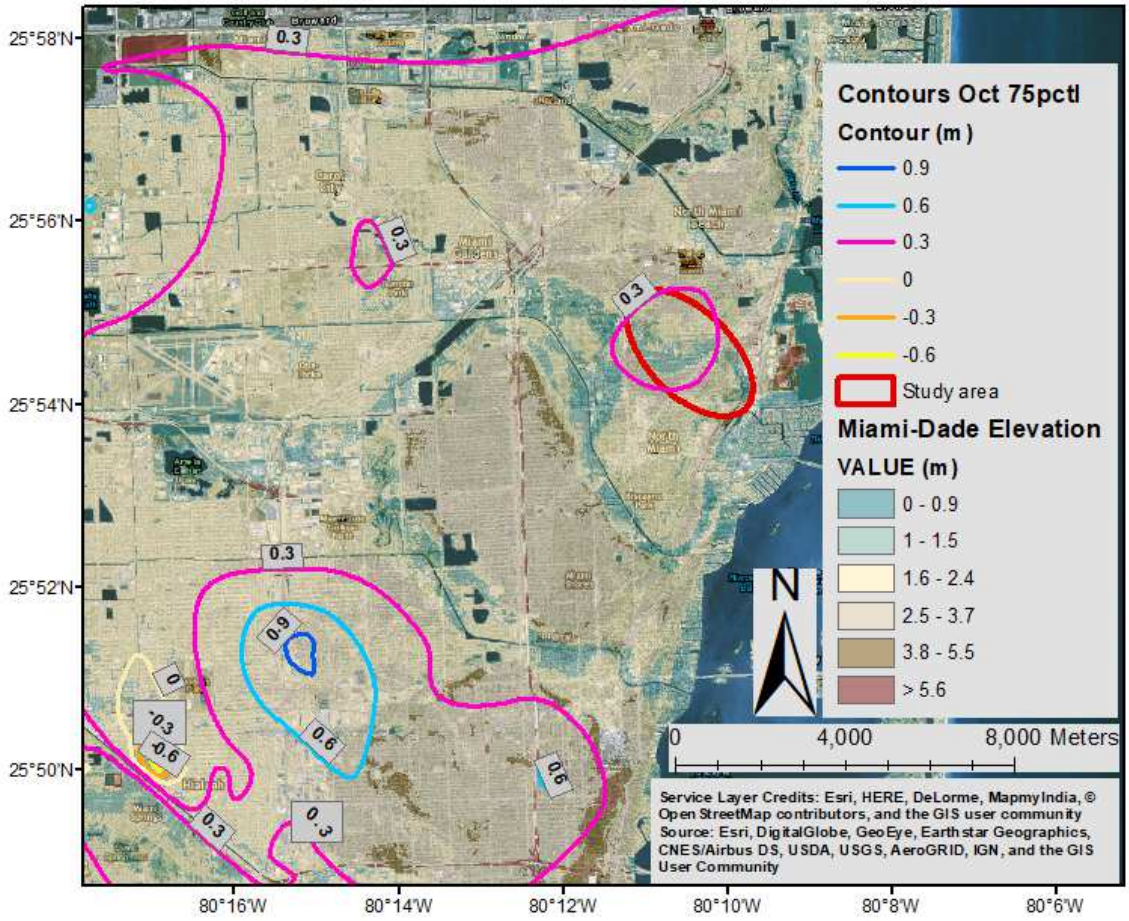

Figure 5. October (end of wet season) 75th percentile 2000-2009 approximate groundwater levels in study area (meters NAVD; adapted from Prinos and Dixon, 2016).

The South Florida Water Management District offer a map-linked database (DBHYDRO) that enables rapid identification and processing of available hydrologic data. Figure 3 shows the two monitoring sites that lie within the sub-region of interest: the well identified as G-852 and the salinity control structure identified as G-58.

There is a substantial water level record for the headwater side of the salinity control structure G-58. Figure 6 shows that water levels at the structure fluctuated mostly between -0.2 and 0.15 m NAVD 88 from 1990 until 2006, when a drop of around 0.2 m occurred. The USACE installed the G-58 structure in 1959 and it was later modified by the South Florida Water Management District. The structure has been inoperable with its gates in the open position for a number of years (U.S. Army Corps of Engineers, 2015); it seems likely that the 2006 change in water level corresponds to this change. Since 2006, water levels appear to show an upward trend, increasing approximately 0.1 m in 10 years (10 mm/y).

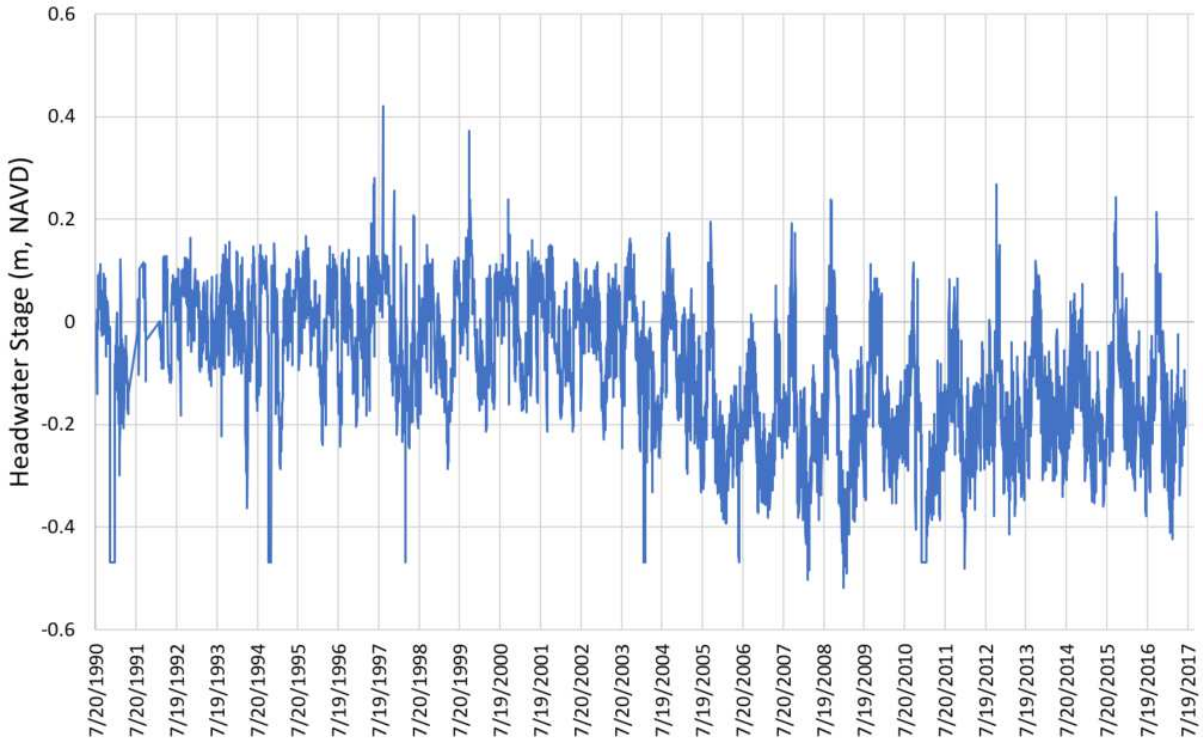

Figure 6. Water level data from the headwater side of salinity control structure G-58.

Comparing the water levels at the G-58 salinity control structure with the nearest tide gage (Virginia Key Florida) reveals that they are often closely coupled, with high and low tides at the structure following those measured at Virginia Key by roughly half an hour (Figures 7 and 8). At most times, the structure headwater levels are slightly higher than the highest tides and slightly lower than the lowest tides. The annual local King Tides occur in late September and October.

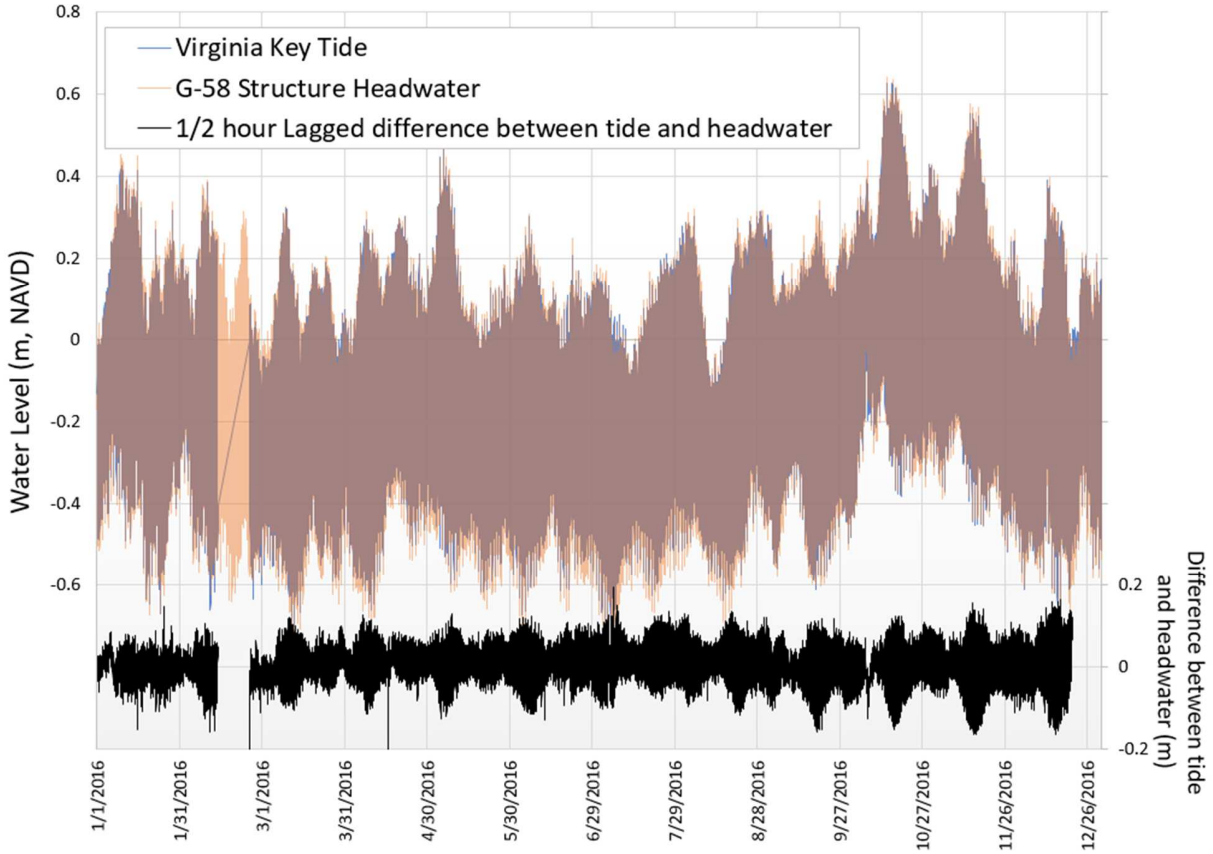

Figure 7. Water level data from the headwater side of salinity control structure G-58 compared with tide data from Virginia Key Florida.

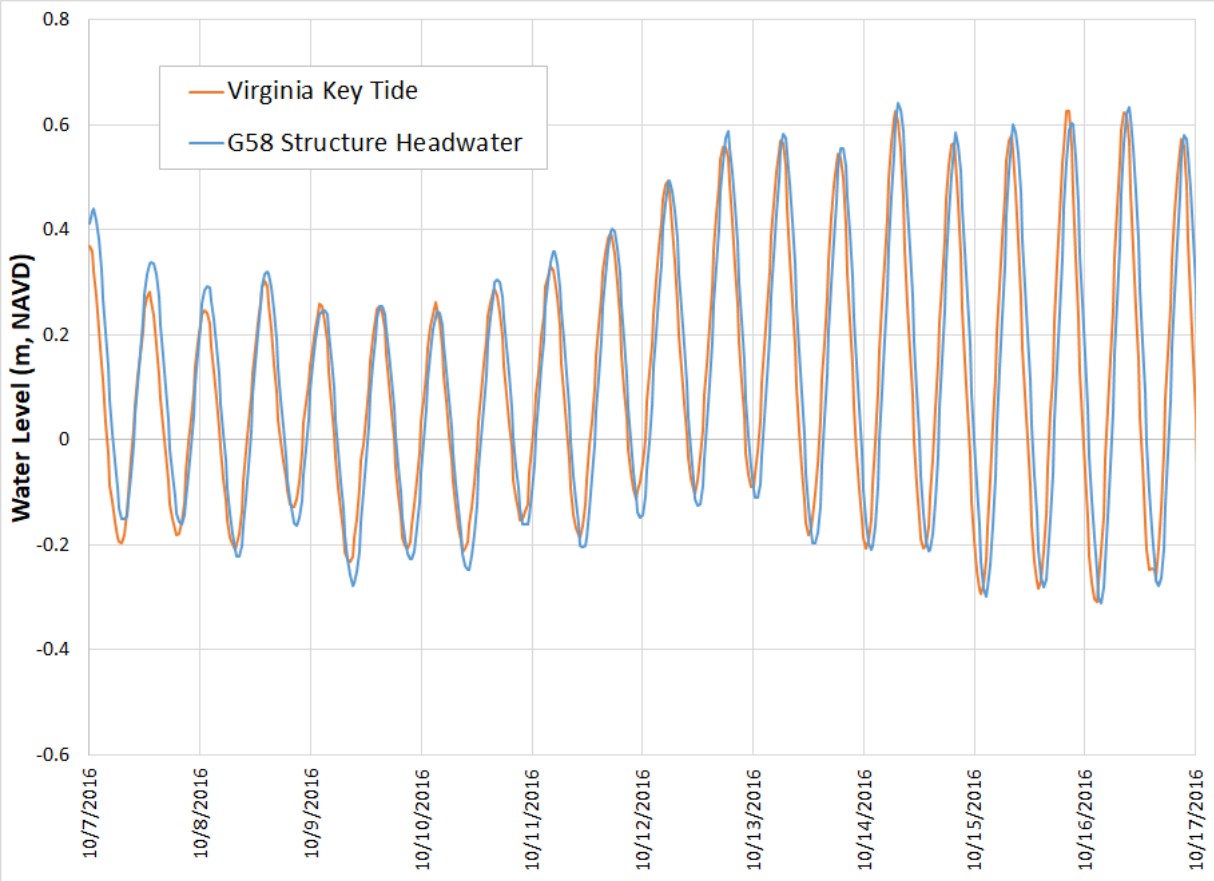

Figure 8. Short term detailed comparison of water level data from the headwater side of salinity control structure G-58 with tide data from Virginia Key Florida.

2.2 Groundwater levels

There is a relatively long history of water levels from well G-852, which is located just west of one of the areas of repetitive-loss properties (Figure 3). The well is 6 m deep. Figure 9 shows mean daily water levels from early May 1959 through September of 1973 and daily maximum water levels from October 1973 through mid-2017. The data indicate an upward trend in water level with time. A linear fit to the data indicates a rate of 2.8 mm/year; this is consistent with long-term Key West tide gage rates of 2.40 +/- 0.15 mm/year (NOAA, 2017) and a possible acceleration in more recent years.

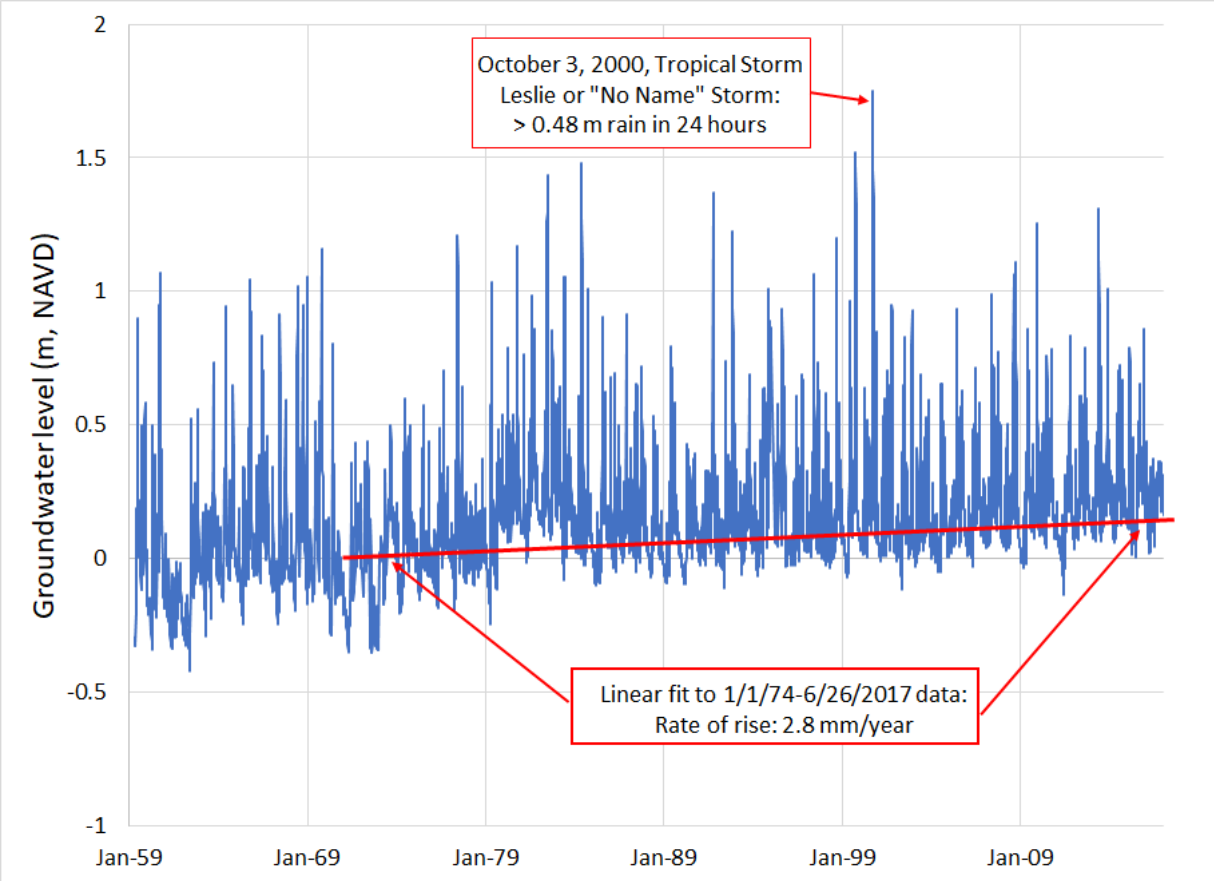

Figure 9. Long-term record of water level data from well G-852 with linear trend.

Water levels have equaled or exceeded 0.9 m NAVD on 102 days and have equaled or exceeded 1.5 m NAVD on three days during the period shown. These exceedances are relevant to and can be evaluated in the context of flooding events. Comparing the water levels with the land surface elevations in Figures 10 and 11 suggests that flooding would have been nearly inevitable in some of the low-lying (<0.9 m NAVD) areas, where repetitive losses have occurred on numerous occasions, and that much more widespread flooding has likely occurred in the area at least a few times (in areas <1.5 m NAVD). In fact, the 3 days of water levels >= 1.5 m NAVD correspond to the highest groundwater levels of nearly 1.8 m, when an October 3, 2000, short-lived tropical storm named Leslie (but frequently referred to locally as the “no-name” storm) dropped more than 48 cm of rain in a 24-hour period in the North Miami area (http://www.northmiamifl.gov/Departments/Publicworks/Floodplaininfo.aspx) causing unprecedented residential property damage and destruction. Adjacent counties were declared major disaster areas (https://www.fema.gov/disaster/1345). Estimated damage was $950 million (Franklin and Brown, 2000). Similarly on May 30, 1984, Markowitz and Stein (1984) reported on widespread flooding in Dade County corresponding to the May 29, 1984 groundwater level of 1.48 m.

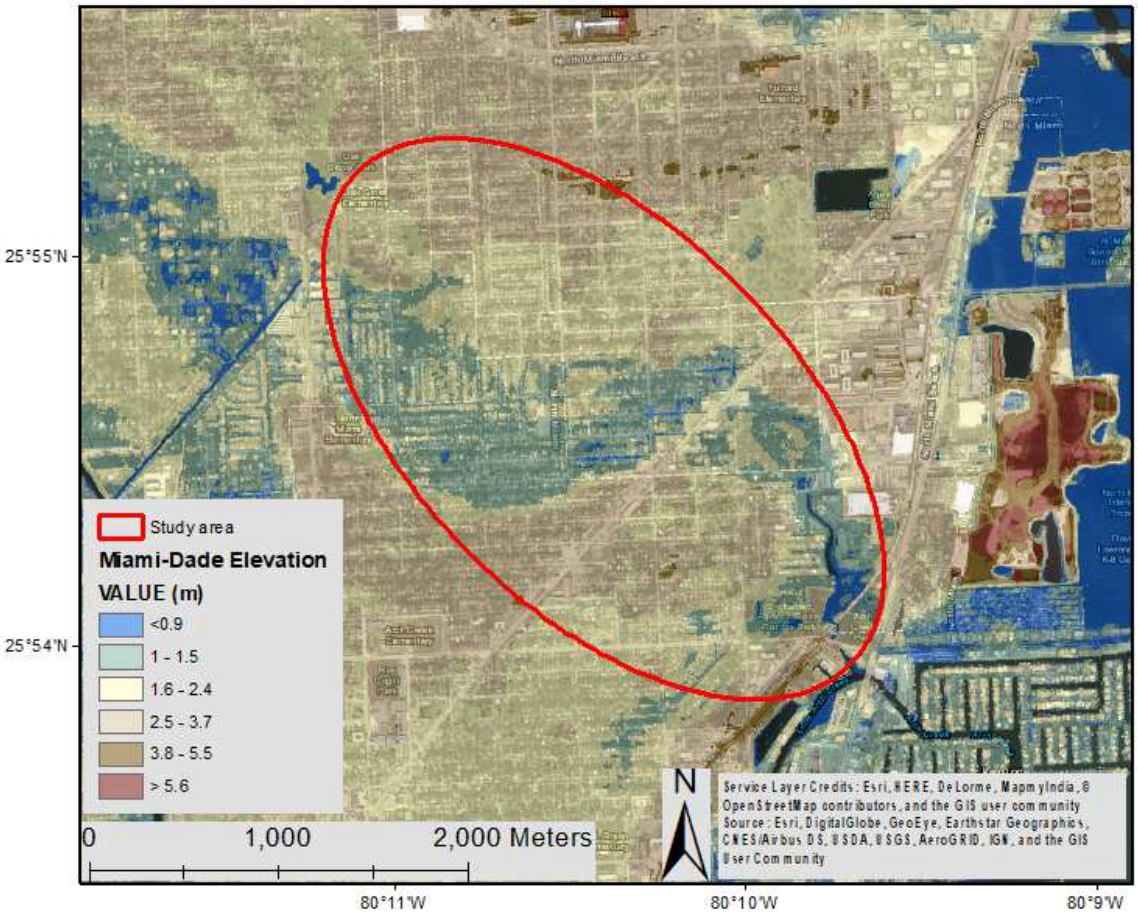

Figure 10. Land surface elevation less than 0.9 m NAVD in dark blue.

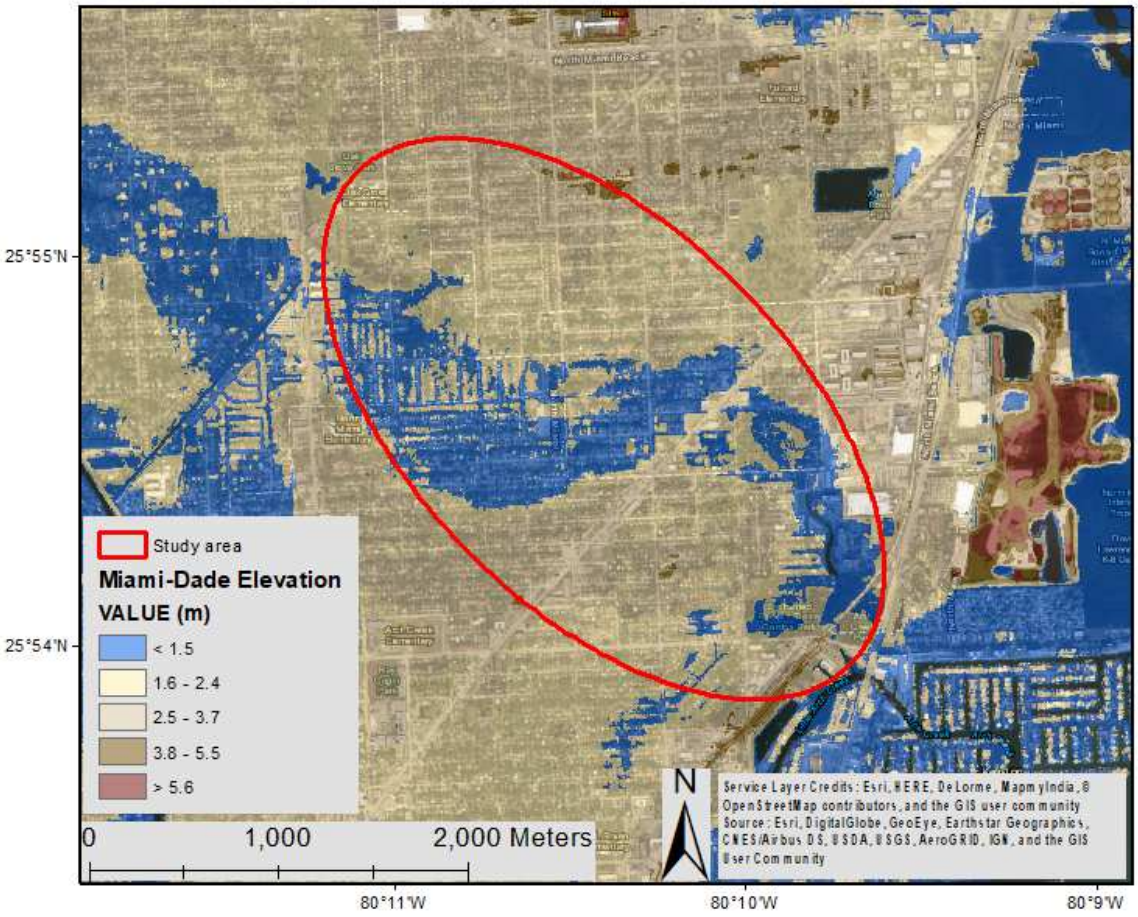

Figure 11. Land surface elevation less than 1.5 m NAVD in dark blue.

This long-term groundwater level record and the continued rise of groundwater over time it shows suggest a simple strategy for estimating the future frequency of groundwater-level-related flooding. Extrapolating the fitted linear trend observed in the 1974-2017 data to the following 43-year period and recycling the 1974-2017 observations by adding the increase due to the trend, enables the frequency of future groundwater-based flooding to be estimated. This estimate should be conservatively low since the selected water level trend is linear, while most sea level rise projections anticipate an acceleration of sea level rise in the future. Figure 12 shows the original 43-year time series of groundwater level elevations at well G-852 and the extrapolated repetition of that series. The horizontal lines show 0.9 and 1.5 m NAVD elevation thresholds. Counts of the exceedances of these levels with and without the extrapolated data are plotted in Figure 12; there is roughly a doubling of the number of days groundwater rises higher than 0.9 m NAVD and a 3-fold increase in the number of days groundwater is higher than 1.5 m, going from the historical 43-year period of 6/27/1974 - 6/26/2017 to the extrapolated period of 6/27/2017 - 6/26/2060.

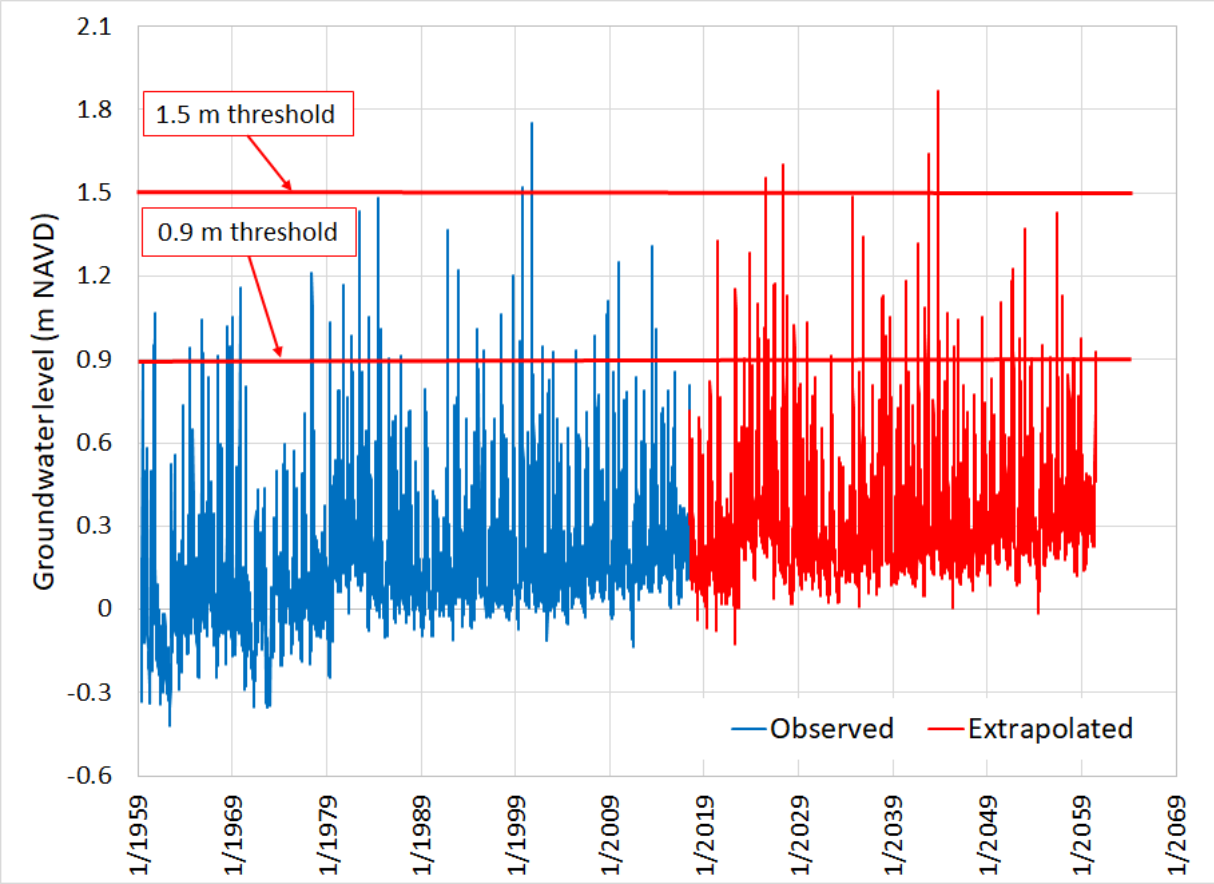

Figure 12. Water level data from well G-852, with 43-year extrapolation to 2060 by recycling 1974-2017 observations increased according to observed trend and lines showing 0.9 and 1.5 m thresholds.

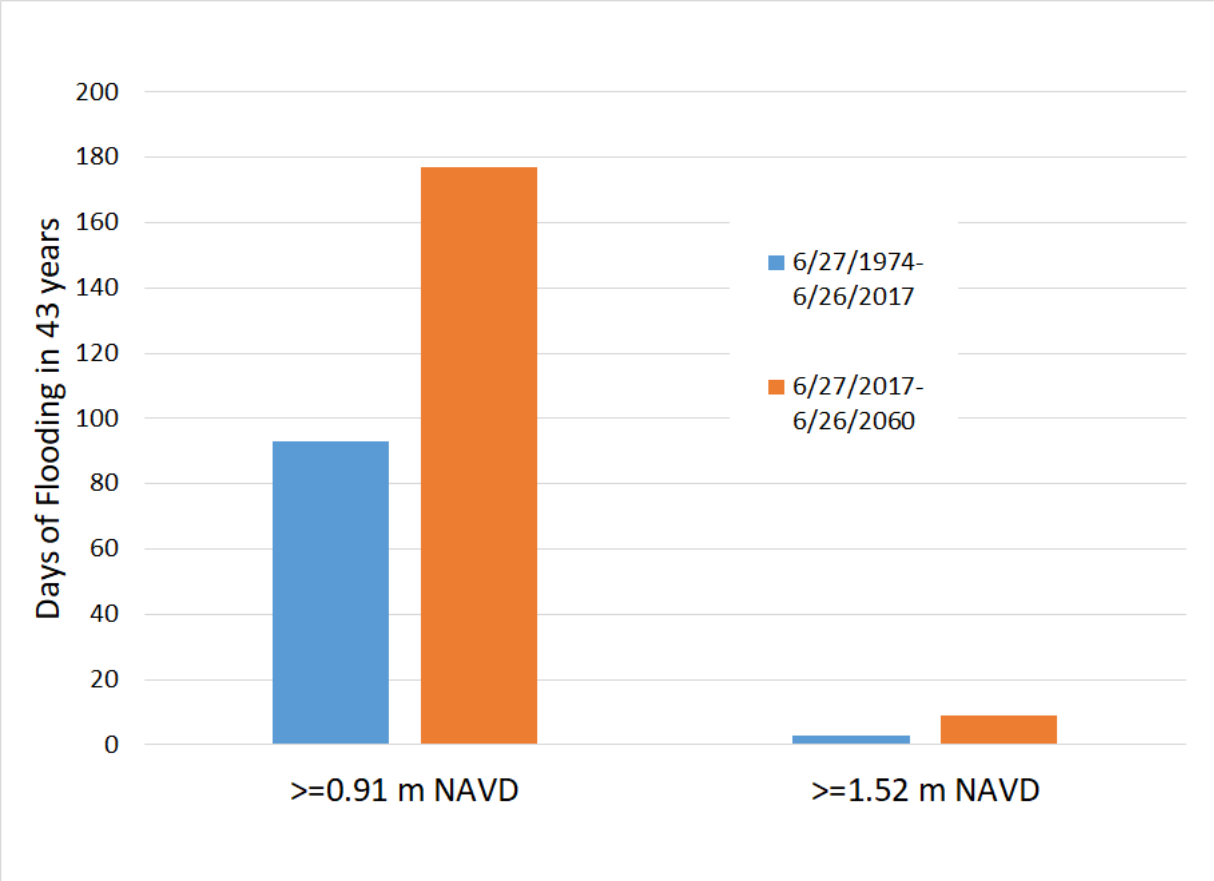

Figure 13. Historical and projected frequencies of well G-852 groundwater levels equaling or exceeding 0.91 m and 1.52 m NAVD based on extrapolation.

3 Test Tidal Impact Model

We created a MODFLOW model to compare MODFLOW results against an analytical model for tidal impacts on groundwater by Jacob (1950); the analytical model is

$$h = h_0 e^{-x\sqrt{\pi S/t_0 T}} \sin\left(\frac{2\pi t}{t_0} - x\sqrt{\frac{\pi S}{t_0 T}}\right) \quad (1),$$

where h is the groundwater head at distance x from the tidal boundary at time t, h_0 is one half of the tide amplitude, T/S is the hydraulic diffusivity, and t_0 is the tide period. We use the same hydraulic diffusivity (501676 m^2/hour) and 12.4 hour tidal period as in Jacob's (1950) example and compute the water level 304.8 m from the tidal boundary. The MODFLOW model is constructed with a total length of 3048 m and discretized into 200, 15.2-m columns. There is one layer and one row. The distal boundary condition is a constant head of 0 m, and the proximal boundary is a time varying constant head that is the tidal stage. Initial condition heads are set to 0 m.

Our results match those of Jacob's example with the water level in the well being 80% of the tide stage with a 25-minute delay. Figure 14 shows the results of the comparison. The

MODFLOW model precisely matches both the magnitude of the peaks and the timing of their arrival as predicted by the analytical solution with a slight difference at the beginning of the simulation that is due to different initial conditions. This provides confidence in our ability to use the numerical model to predict tidal fluctuations of head in the aquifer.

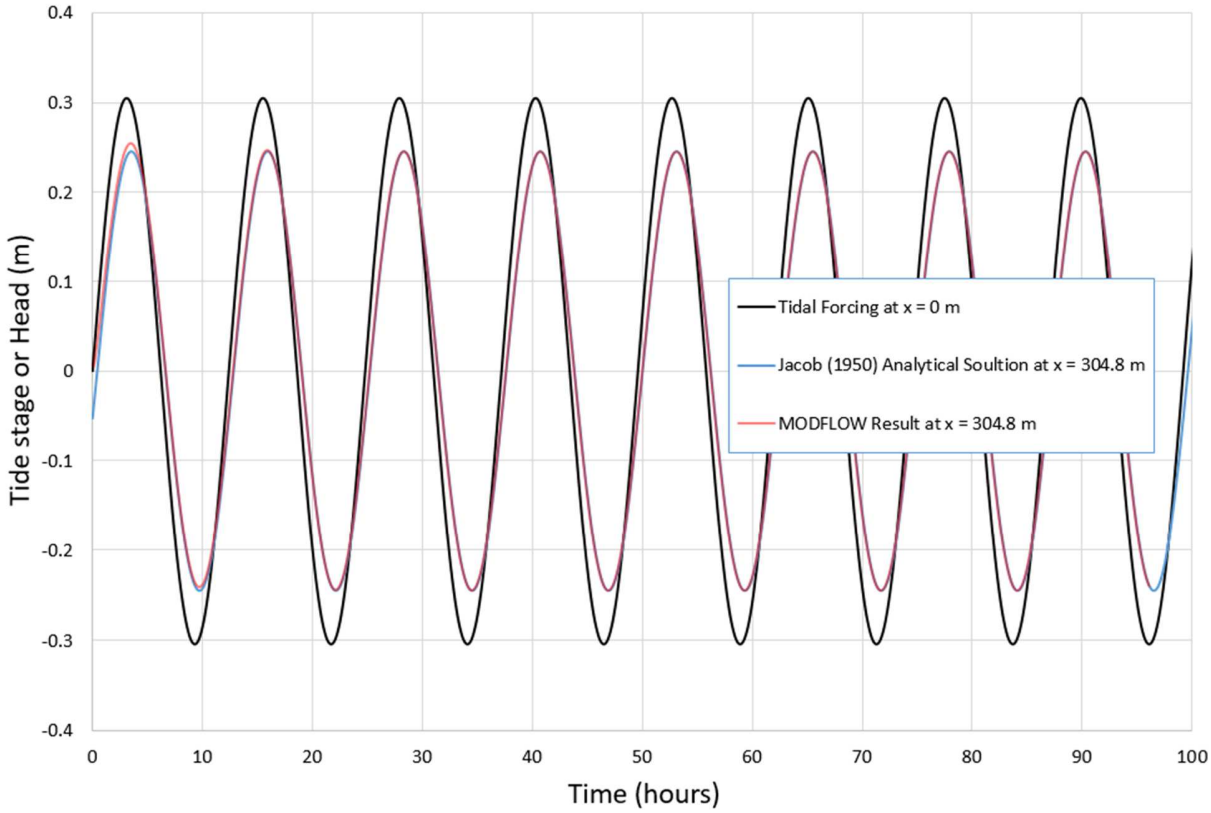

Figure 14. Comparison of Jacob (1950) analytical solution and MODFLOW model results.

4 Arch Creek Groundwater Model

A 1-D groundwater flow model was constructed using the MODFLOW and the graphical user interface ModelMuse (Winston, 2009). Figure 15 shows the location of the model and its boundary conditions. The model is composed of 100 30.5-by-30.5-meter cells and hence has a total length of 3048 m. The aquifer thickness is assumed to be 30.5 m. Given the relatively small changes in water level compared to the thickness, the aquifer can be mathematically treated as confined with little loss of fidelity. The model time step is chosen as 30 minutes to permit quality resolution of the tidal cycles. Longer times led to aliasing. The tidal frequency is ⅙ hours^{-1} and the Nyquist frequency needed to minimally resolve the frequency of the tidal signal is twice that at ⅓ hours^{-1}. Our sampling/simulation rate of 6 times the Nyquist frequency (2 per hour or ½ hour time steps) ensures good reproduction of the tidal fluctuations.

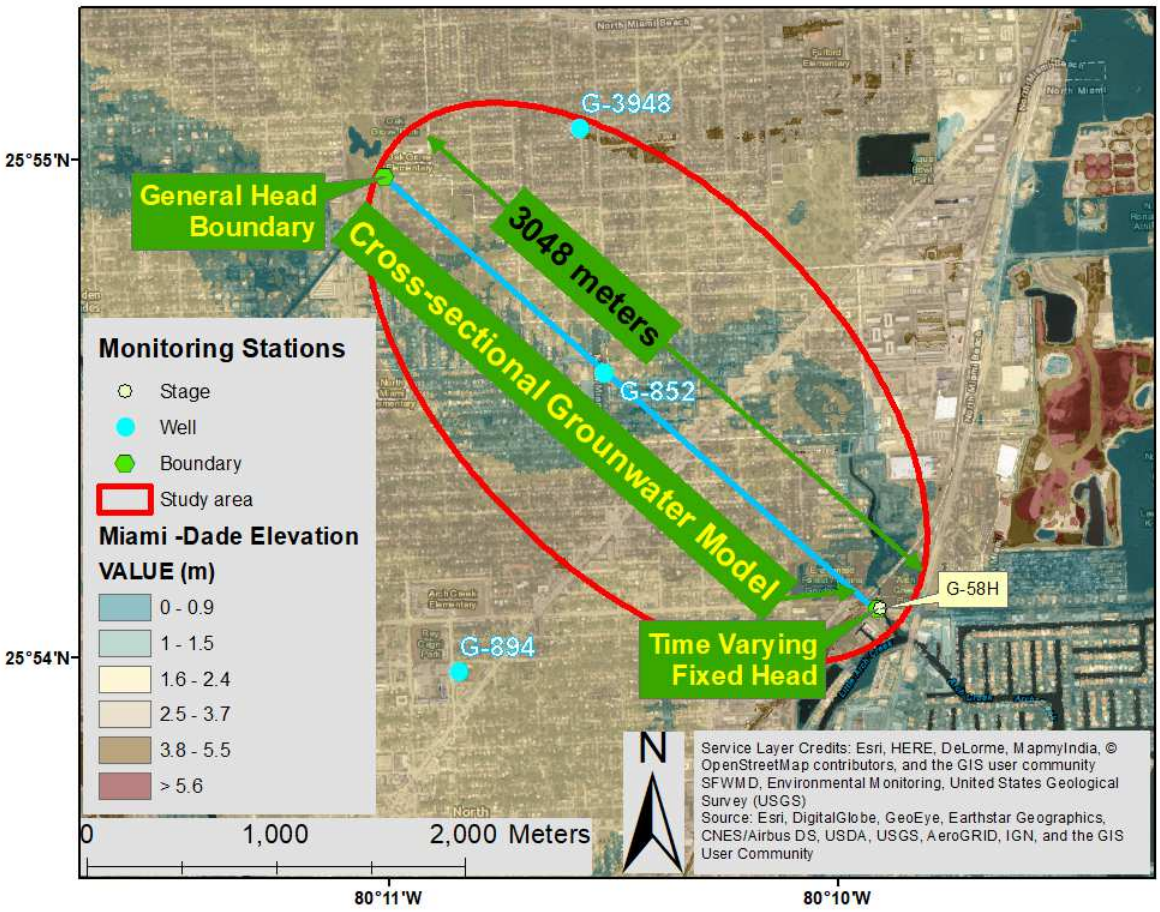

Figure 15. Orientation and boundary conditions of 1-D MODFLOW model.

4.1 Precipitation Data

The rainfall data selected for this model were measured by Next Generation Radar (NEXRAD) because this observing system has high temporal and spatial resolution for rainfall in the studied area. Pathak (2004) described the system in detail. The rain grid resolution is 2 km x 2 km. The amount of the rain is measured by NEXRAD using reflectivity with calibrated algorithms. SFWMD collects rain data from 5 radar sites (Tampa, Melbourne, Jacksonville, Miami, and Key West). Two methods are used to derive the rainfall estimates. The first method is the Z-R relationship where Z is radar reflectivity data presented in polar coordinates, and R is rain intensity data. This method uses $Z=200R^{1.6}$ (Marshall Palmer), $Z=130R^{2.0}$ (winter stratification), or $Z=300R^{1.4}$ (summer convective storms). The second method employs an empirical look-up table that uses upper air parameters, reflectivity values, and observed rainfall. Finally, the rainfall data are adjusted using gage methods, including uniform G/R ratio, uniform G/R ratio within calibration zones, Brandes method, National Weather Service (NWS) mean-field bias, and NWS P1 method (Pathak, 2004).

Rainfall data were available at 15-minute intervals from the South Florida Water Management District's (SFWMD) NexRad-based database, which are near real-time data, received by SFWMD from 80 telemetry stations and rain-gage adjusted every 15 minutes. The rainfall data were downloaded in units of inches from four rain grids that overlap the model area, 10044041, 10044042, 10044515, and 10044516, and the average of the rainfall in these grids was calculated.

The following algorithm was used to re-cast the 15-minute rainfall record into half-hour time steps in a way that conserved the total amount of rainfall:

$$P_{0.5adj} = P_{0.25}/2 + P_{0.5} + P_{0.75}/2 \qquad (2),$$

where the subscripts represent the mass-conserving adjustment into ½ hour steps (0.5adj), the rainfall during the 15-minute period preceding the selected ½ hour step (0.25), the rainfall during the 15-minute period represented by the selected ½ hour step (0.5), and the rainfall during the 15-minute period following the selected ½ hour step (0.75).

4.2 Calibration and Validation

All of the year 2015 data were selected for calibration and all 2016 data were used for validation. These years had anomalously high dry season rainfall (SFWMD, 2016), though they did not include more extreme rainfall event such as those generally associated with tropical storms or hurricanes.

The ModelMate (Banta, 2011) interface between ModelMuse (Winston, 2009) and the parameter estimation software UCODE (Poeter et al., 2014) were used to estimate the hydraulic conductivity and storativity for 4 fixed recharge rates that represented 25, 50, 75, and 100% of rainfall.

4.3 Boundary Conditions

The downstream boundary is set to the headwater stage at the G-58 structure, which has been open for several years and often closely follows the tides.

There is ambiguity about the upstream/inland boundary due to the lack of an obvious boundary in that area. Spur Canal No. 4 (Figure 2) might be an appropriate boundary, but it appears that there are no stage data for that reach of the canal at this time. The headwater data from the S-28 structure about 5 km downstream may be the closest available stage data but are too far downstream to be relevant for the upstream model boundary.

The three basic possibilities for this boundary include a constant head, a closed boundary, and a head-dependent flux boundary (a General Head Boundary in MODFLOW terminology). Each

type of boundary has advantages and disadvantages and we experimented with each type as described below.

4.3.1 Constant head boundary

The constant head boundary head has to be estimated and, in the simplest case, it is fixed at a single value over time. We selected a boundary head to be consistent with the initial condition, which is based on a linear fitting of the annual average downstream stage at the G-58 structure (around -0.15 m NAVD in 2015 and 2016) and the observed starting head at well G-852. The initial condition is computed as a linear function of (negative) distance Y_prime (m) from the upstream boundary as

Head = (head at G-852 - average G-58 head)/(1524 m) * Y_prime + upstream boundary head, (3)

where we first solve for the upstream head using G-852 and G-58 starting values. For example, on January 1, 2016, the head at G-852 was 0.19 m and the average head at G-58 was taken as -0.15 m. Inserting these values into (3) as

-0.15 = (0.19 - (-0.15)) /1524 * (-3048) + upstream boundary head

permits solution for the upstream boundary head as 0.52 m.

We solved for the upstream heads as 0.49 m and 0.52 m for the 2015 and 2016 model runs respectively. Using the constant head boundary condition provided the best model calibration fit to the G-852 observations with correlation coefficient 0.93. The head profiles showed that this boundary permitted the development of a groundwater divide where water flowed towards the sea on one side and in the opposite direction towards Spur Canal No. 4 on the other side. This is consistent with USGS maps of seasonal water levels (Figure 5).

Table 1 shows the correlation matrix for the model parameters. The correlation of the hydraulic conductivity and storativity is low (for the fixed recharge as described below) and indicates good independent estimation of the two model parameters.

Table 1. Parameter correlation matrix for constant head boundary

	Storativity *S*	Hydraulic Conductivity *K*
Storativity *S*	1	0.057
Hydraulic Conductivity *K*	0.057	1

4.3.2 No-flow boundary

Also consistent with Figure 5, hydraulic gradients on the inland end of the model are expected to be small and stagnation (zero gradient) points may exist. This argues for consideration of a closed no-flow boundary. The closed boundary was simpler because no head had to be estimated. It had the additional advantage that the head at the boundary could change freely in response to recharge and groundwater flow in the rest of the model; only the gradient at the boundary is constrained. The head changed significantly from more than 0.6 to nearly 0 m NAVD over the course of a year. The only outlet for water in this model is drainage to the tidal boundary, and drainage through the model is a relatively slow process. Very low heads in the simulation were the result of drainage of the groundwater system during a period of limited recharge, and contributed to a reduced ability to calibrate to the observed heads. The correlation coefficient (0.83) between the observed and simulated heads was considerably lower than it was for the constant head boundary. The parameter correlation matrix in Table 2 indicates an undesirable much higher correlation between the estimated model parameters.

Table 2. Parameter correlation matrix for no-flow boundary

	Storativity *S*	Hydraulic Conductivity *K*
Storativity *S*	1	-0.33
Hydraulic Conductivity *K*	-0.33	1

4.3.3 General head boundary

The final boundary condition considered is the General Head Boundary of MOFLOW. The boundary can be written as

$Q = C\ (h - h\_ref)$,

where Q is the flow, C is the conductance, h is the head, and h_ref is a reference head. The flow increases as the head at the boundary departs from h_ref. Note that when C is 0, there is no flow and the boundary is identical to a closed boundary. When C is very large, large flows can occur to ensure that the head remains essentially equal to h_ref and the boundary takes on the character of a constant head boundary. This continuum of behaviors from closed to constant head has the advantage (shared with the closed boundary) that the simulated head can change in response to model conditions and the advantage (shared with the constant head boundary) that inflows and outflows through the boundary are possible. The disadvantages are that a reference head and a conductance have to be selected. The conductance can theoretically be computed from the interfacial area between model cells ($w * d$), the distance between model cells centers over which the head change occurs (Δx), and the hydraulic conductivity (K): $C = K\ w\ d/(\Delta x)$. In our model, the cells are 30.5 m wide and 30.5 m deep, and have a separation distance of 30.5 m. The hydraulic conductivity is a calibration parameter but is on the order of 30.5 m/hour. Thus the conductance can be estimated as 930 $m^2\ hr^{-1}$. This is a high value in the context of our model and means that the boundary will behave much like a constant head

boundary would behave. The correlation coefficients for the model fit to the observations and between the model parameters are essentially the same as those of the constant head boundary and are described below.

4.4 Calibration

Calibration is the process of fitting the model to observations by adjusting model parameters until the best possible fit is obtained. We chose to work with the General Head Boundary in the final calibration.

The governing equation for the model is the two-parameter 1-dimensional transient groundwater flow equation

$$\frac{\partial h}{\partial t} = \frac{T}{S}\frac{\partial^2 h}{\partial x^2} + \frac{R}{S} \quad (4).$$

Given the 2 parameters (*T/S* and *R/S*) and the available calibration information (a time series of observed maximum daily head values from a single monitoring well), we can never estimate *T*, *R*, and *S* values separately unless one of them is known. Our strategy was to fix the recharge as one of 4 different fractions of precipitation and proceed with the parameter estimation process. Given the high permeability of the Biscayne Aquifer, its outcrop at the surface, and the prevalence of dry well drainage where stormwater is directed to the aquifer, this simplistic treatment of recharge was considered adequate.

Tables 3 and 4 show the results. Starting estimates of *K* and *S* were 50% of preliminary manual calibration values to permit UCODE to find optimal solutions. The correlation coefficient for the model fit to the G-852 observations is 0.93 in all cases. The ratio *K/S* (which is proportional to *T/S*) is nearly constant for all of the different recharge fractions, pointing out the non-independence of the parameters and the resulting non-uniqueness of the *K* and *S* parameters in this particular case.

Table 3. Calibration results for different recharge values

Run	K (m/s)	S (-)	K/S (m/s)
100% recharge, S_0.05, H_K_50, Tol_0.05	8.89×10^{-3}	1.27×10^{-5}	6.05×10^{-2}
75% recharge, S_0.05, H_K_50, Tol_0.05	6.67×10^{-3}	9.31×10^{-6}	6.04×10^{-2}
50% recharge, S_0.05, H_K_50, Tol_0.05	4.45×10^{-3}	6.27×10^{-6}	6.03×10^{-2}
25% recharge, S_0.05, H_K_50, Tol_0.05	2.19×10^{-3}	3.13×10^{-6}	5.99×10^{-2}

Table 4. Parameter correlation matrix for calibration runs with general head boundaries at two recharge fractions

$R = 0.75\ P$	Storativity S	Hydraulic Conductivity K
Storativity S	1	0.056
Hydraulic Conductivity K	0.056	1
$R = 0.25\ P$		
Storativity S	1	0.056
Hydraulic Conductivity K	0.056	1

The calibration run results with 75% of NexRad rainfall as recharge are shown in Figure 16. The calibration is very good at fitting most of the highest peaks (with a notable exception of a peak in response to an extended period of rain in mid- to late-September where the model underestimates the peak by 0.19 m). From June and part of the way into August, the model overpredicts the relatively low observed heads, though the difference is always less than 0.15 m.

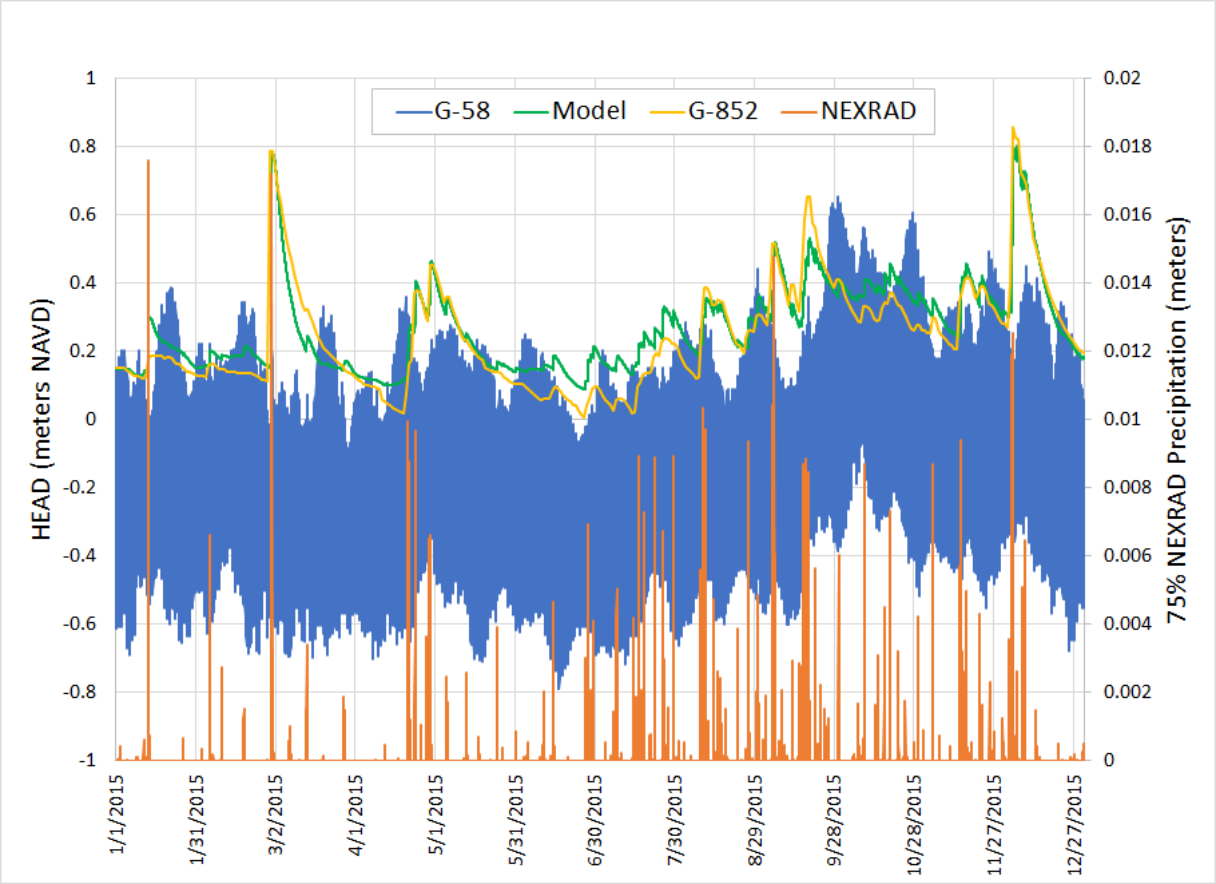

Figure 16. Results of MODFLOW/UCODE model calibration to 2015 G-852 observation well data.

It is useful to look at cross sections of the head field. In June, shortly after the end of the normal November to April dry season, the head decreases steadily from the northwest end of the model to near the G-58 structure on the southeast end of the model (Figure 17). Following the heads over a tidal cycle shows that the modeled tidal influence does not extend more than 610 m inland from the structure and that on this date, when the tidal range is about 0.31 m, appreciable effects (0.15 m change) do not extend more than about 305 m inland from the structure.

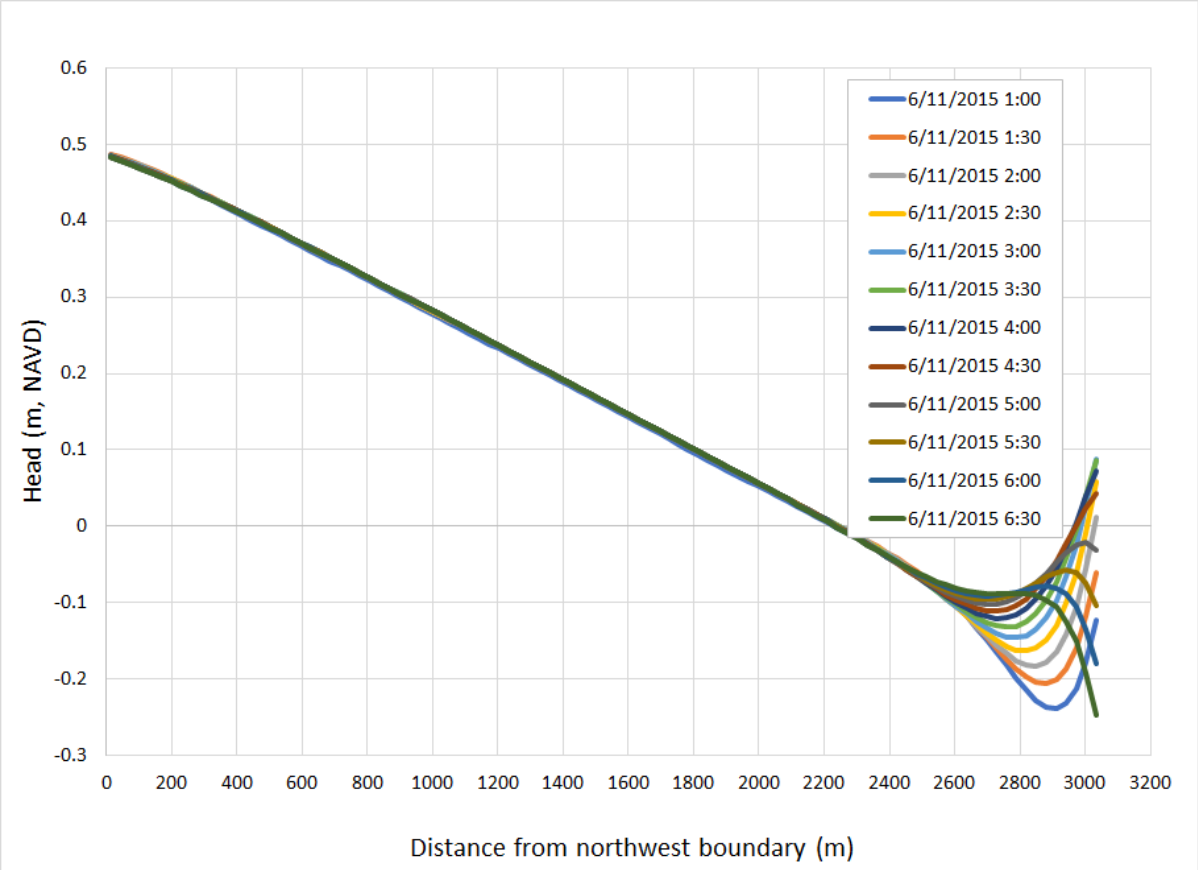

Figure 17. Cross-sections of simulated head from northwest to southeast (at G-58) on June 11, 2015.

In September on one of the days of the local King Tide (September 29th) groundwater levels were generally higher by more than 0.15 m and the tidal range was nearly 0.91 m, but there was similarly little inland penetration of the tidal signal (Figure 18). This date followed an extended period of rain in mid- to late-September that caused mounding of the modeled groundwater head between the model boundaries and led to northwestward flow toward the General Head Boundary over about 305 m of the model. This is consistent with USGS maps of seasonal water levels (Figure 4) and a conceptual model that includes groundwater flow towards Spur Canal No. 4 (Figure 2) in response to lowering of the head by drainage.

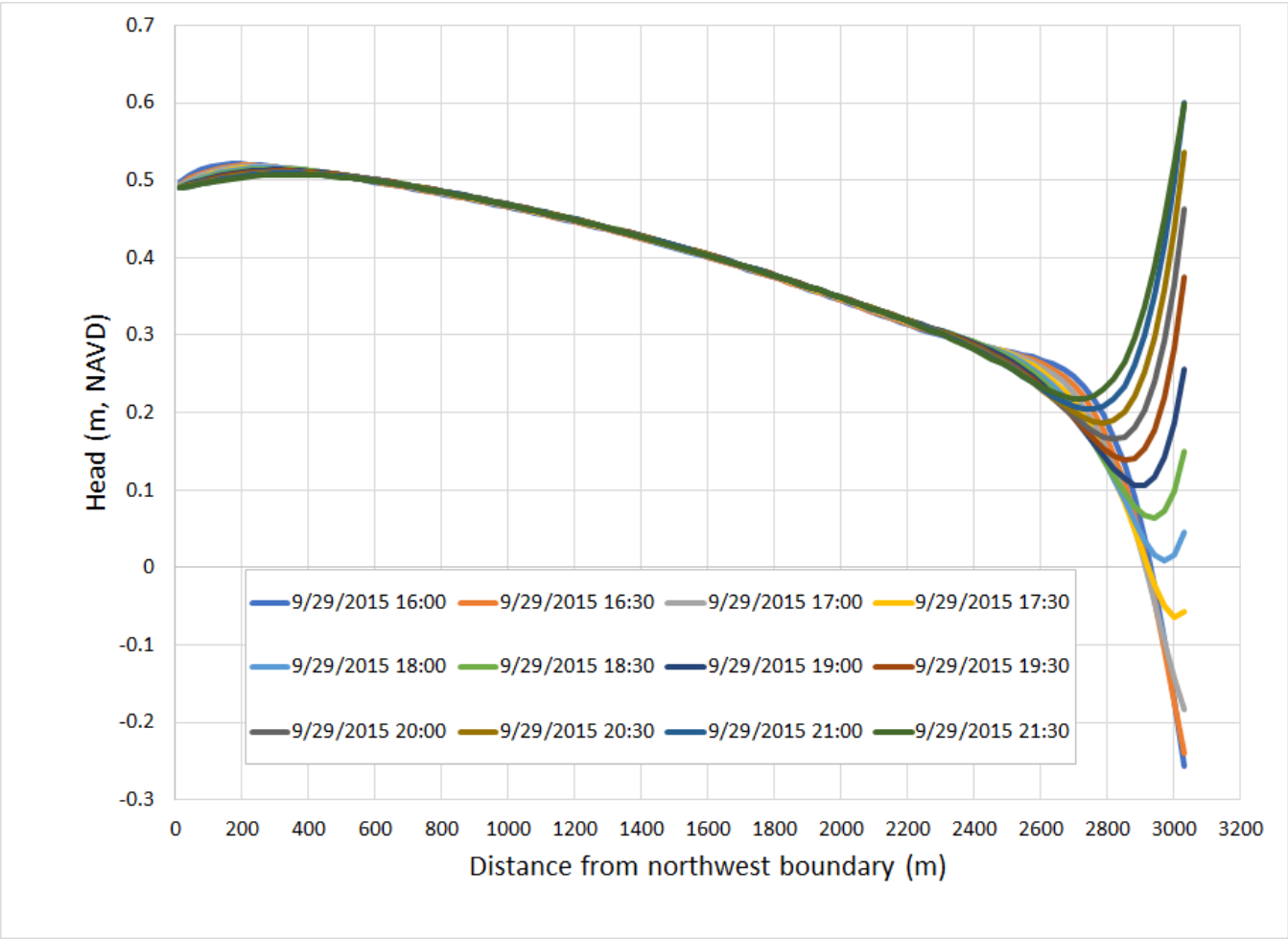

Figure 18. Cross-sections of simulated head from northwest to southeast (at G-58) on September 29, 2015.

4.5 Validation

In validation, the model parameters estimated via calibration are used to simulate (without fitting) another time period with observations that are compared to model estimates for the purpose of testing of the model and its parameters. The results of the validation run for 2016 rainfall and the well G-852 head data are shown in Figure 19. The model over-predicts the observed head values by as much as 0.2 m, though predictions are generally much better in the January through mid-March and May through December time periods, which includes both South Florida's wet season and its King tides. The reasons for the departure of the model from the observations in mid-March through the end of April are unknown but might be due to active drainage as discussed below.

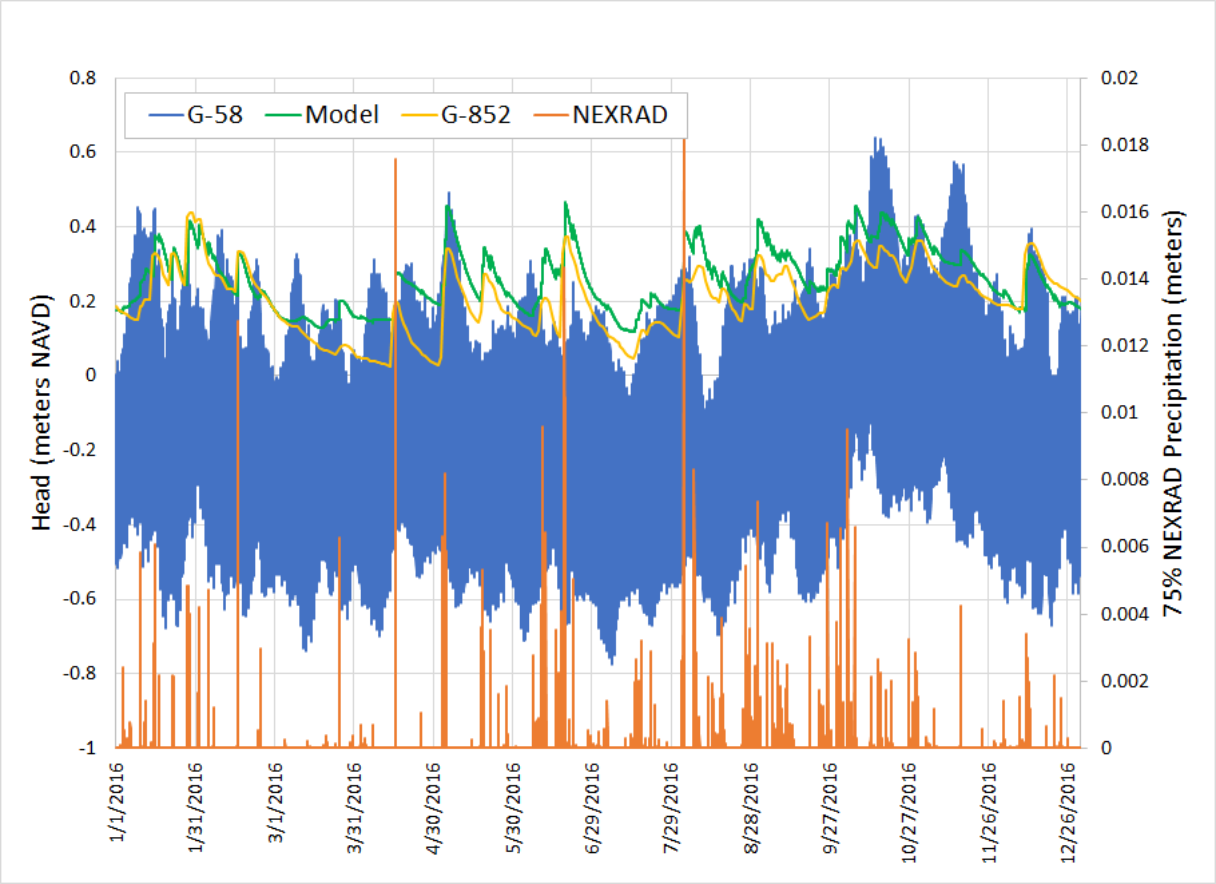

Figure 19. Validation of model with 2016 observations at G-852.

For comparison to our model calibration and validation results, Figure 20 shows results from the daily time step model developed by the U.S. Geological Survey (Hughes and White, 2016), which is the principal model used for county-scale planning. The Hughes and White (2016) model covered the entire urban area of Miami-Dade County at a horizontal spatial resolution of 500 m and incorporated many additional processes than those we use in our model -- in particular, explicit surface water and land cover/ET-based recharge. Its calibration sought to balance agreement with many more observations than we consider here.

During both the calibration and validation time periods, the Hughes and White (2016) model results are often almost 0.3 m higher than the observations at G-852, except that peak groundwater levels are usually underestimated up to as much as 0.6 m. This underestimation would have appreciable impact on the model's ability to predict flooding from water table rise in the Arch Creek area.

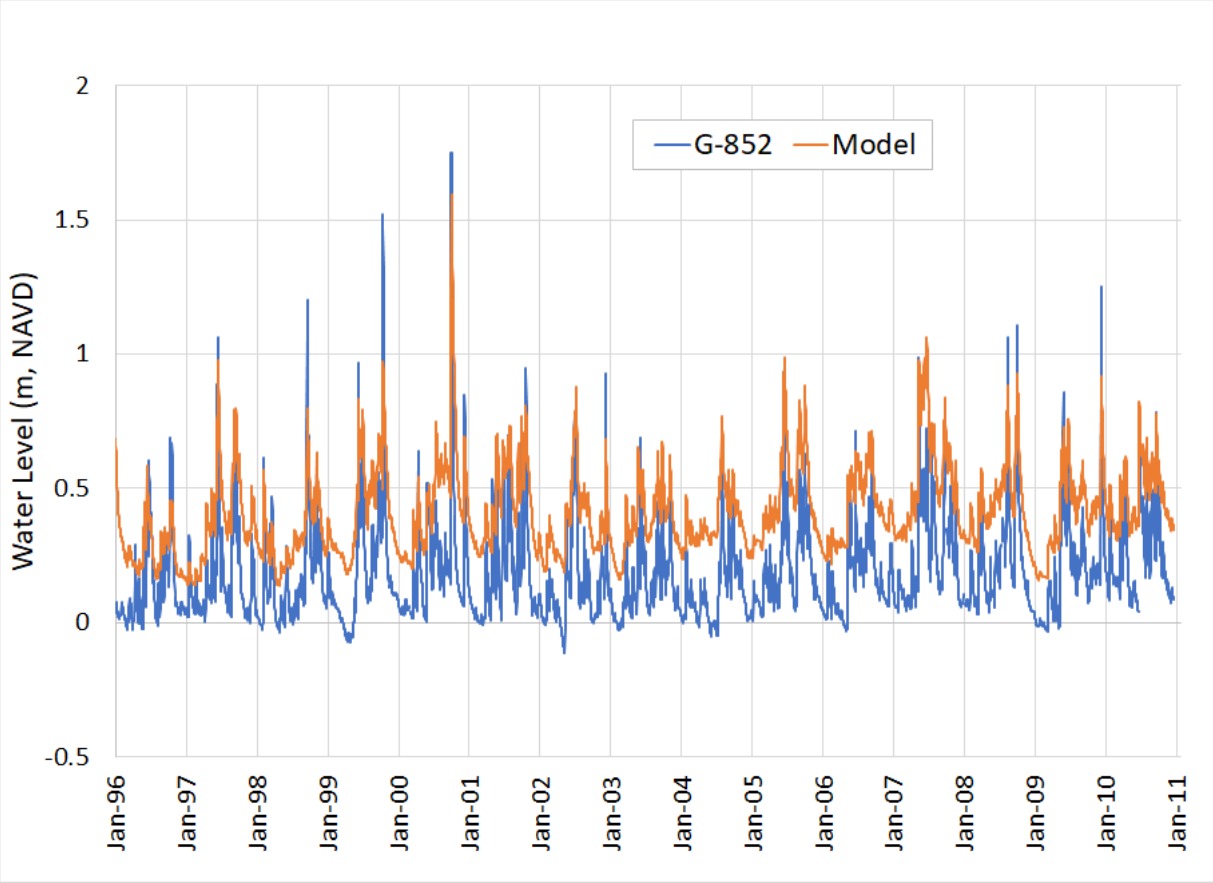

Figure 20. Calibration and validation of USGS model (Hughes and White (2016) to observations at G-852.

5 Future Projections

5.1 Projection of 2060 conditions

The calibrated and validated model was used to estimate groundwater and groundwater-related flooding conditions in 2060. The projection of future conditions followed a simplified scenario approach as outlined by Obeysekera et al. (2014), who developed a set of six climate and sea level scenarios for use in assessing possible hydrologic impacts on the greater Everglades region using the South Florida Water Management Model. The scenarios included a 1.5 °C increase in temperature (which would affect evapotranspiration), ±10 % change in precipitation, and a 0.46 m increase in sea level for a 50-year (2060) horizon.

5.1.1 Sea Level Rise and Tides

Based on the U.S. Army Corps of Engineers Sea-Level Change Curve Calculator (2017.42, http://www.corpsclimate.us/ccaceslcurves.cfm), we adopt the USACE High curve for the Miami Beach tide gauge. This indicates a 0.61 m rise in sea level between 2010 and 2060 (Table 5).

Table 5. Estimated Relative Sea Level Change
from 2010 To 2060 from U.S. Army Corps of Engineers Sea-Level Change Curve Calculator
8723170, Miami Beach, FL
NOAA's 2006 Published Rate: 0.000239 m/yr
All values are expressed in meters

Year	USACE High
2010	0
2015	0.04
2020	0.08
2025	0.12
2030	0.17
2035	0.23
2040	0.30
2045	0.37
2050	0.44
2055	0.52
2060	0.61

We add this 0.61 m rise to the 2016 tidal boundary data from structure G-58 to create a new boundary for the simulation of future conditions.

5.1.2 Northwest Boundary Condition

Given the observation (Figure 8) that groundwater has been rising at approximately the same rate as sea level, we add the 0.61 m of projected 2060 sea level rise to the General Head boundary condition on the northwest end of the model for the 2060 simulation.

5.1.3 Rainfall

As in Obeysekera et al. (2014), we increase each ½ hour 2016 rainfall amount by 10% for the simulation of possible 2060 conditions. This translates directly into 10% additional recharge via our simple approach. An alternative approach to using the 10% precipitation increase is to directly utilize climate model output, but products that simultaneously meet the spatial and temporal resolution scales to drive our model are currently lacking as discussed below.

5.1.4 2060 Model Results

Figure 21 shows the results of the 2060 model run. Here “Model” refers to the groundwater levels at the location of G-852 and Row 60 and Row 80 refer to the levels 1829 m and 2438 m from the northwest end of the model (1219 and 610 m from the G-58 structure respectively). Overall groundwater levels at the G-852 location increased from about 0.3 m NAVD on average to nearly 0.9 m NAVD consistent with the 0.61 m changes in the boundary conditions. The 10% increase in recharge also results in a slightly more ‘flashy’ time series of model predictions.

Predicted water levels at model rows 60 and 80 are presented to test if the tidal influence might extend farther inland than it does in the calibration and validation runs. The conclusion is that there is a definite influence of the tide that is damped and offset in time going inland, as expected. The tide peak in mid-March is accompanied by a 3-6 cm rise in groundwater level at Row 80 in the near-absence of rain and recharge. At Row 60, the groundwater peak is more subdued with an amplitude of perhaps 1.5 cm and is shifted to a later time. This diminution of response and the larger time shift are even more pronounced at Row 50, the location of well G-852.

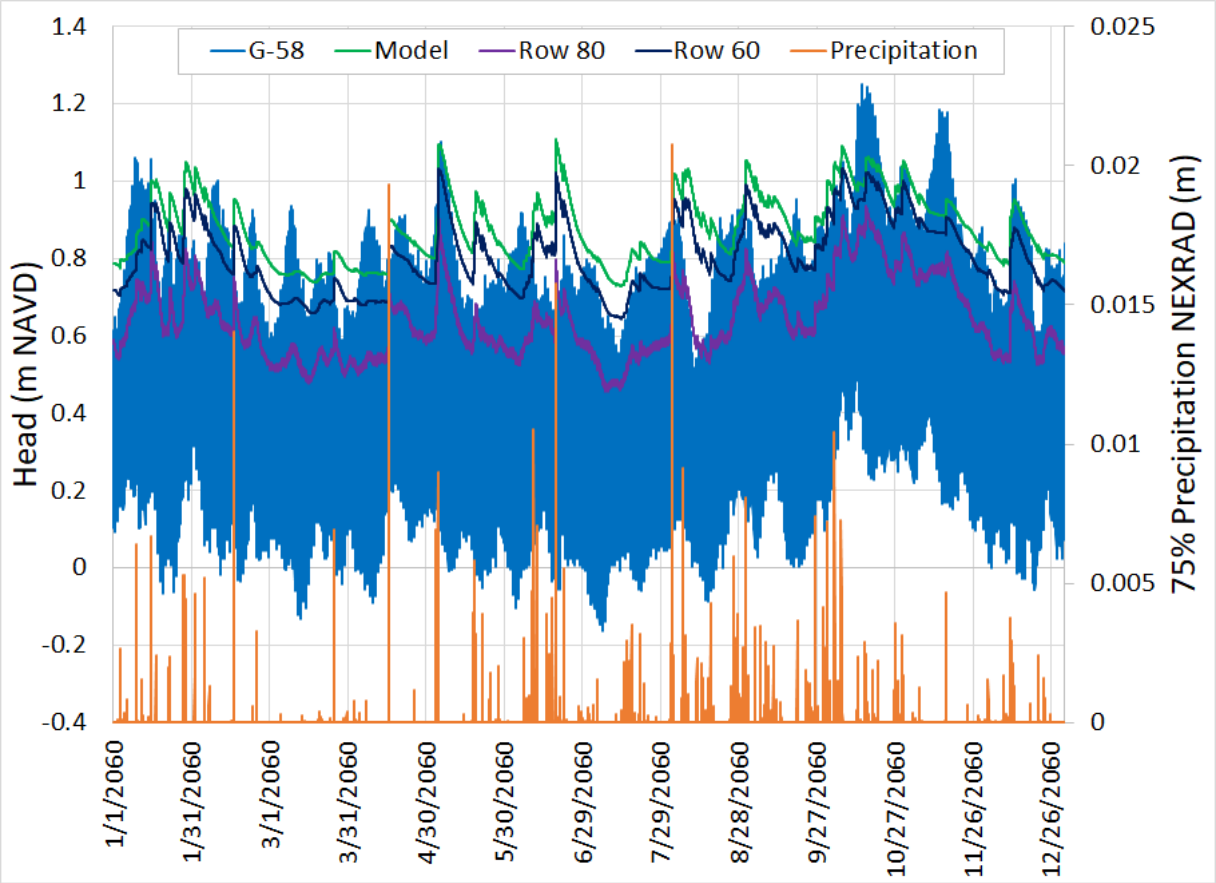

Figure 21. Projection of Arch Creek groundwater model to 2060 scenario of 0.61 meters sea level rise and +10% precipitation. ‘Model’ refers to the prediction at the site of G-852, Row 60 is the prediction at 1829 meters from the northwest model boundary and Row 80 is the prediction at 2438 meters from the northwest model boundary.

To assess the spatial locations of likely flooding during periods of high groundwater, we collect land surface profiles from 5 traverses of the study area as shown in Figure 22. From northeast to southwest, these traverses (Elevation 1 through Elevation 5 respectively in Figures 22 and 23), pass through the low lying lower and upper portions of the ancestral floodplain.

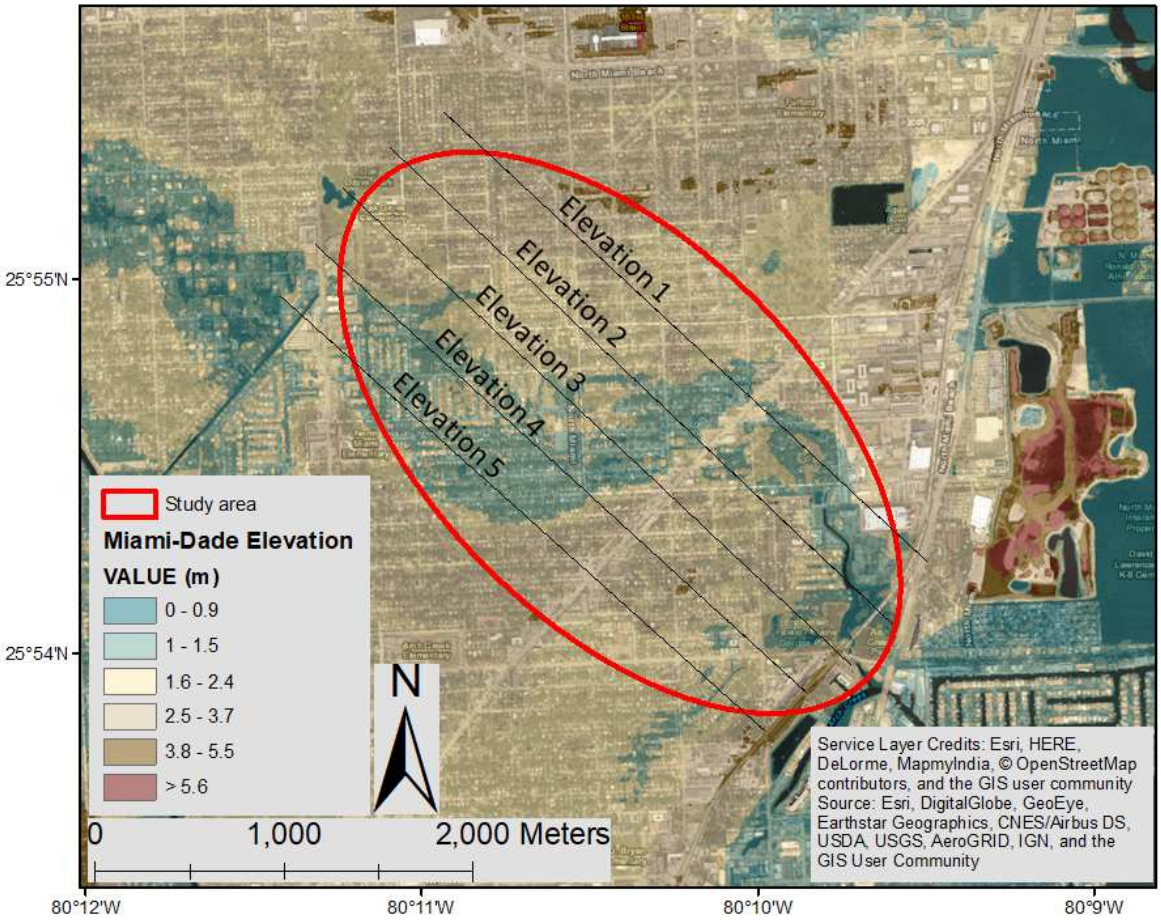

Figure 22. Locations of land surface profiles.

These profiles are plotted along with the profile of the projected October 16, 2060 groundwater elevations over a tidal cycle on Figure 23. They reveal the most likely areas of flooding as southeast of well G-852 between 400 and 600 m from the northwest model boundary, between 1000 and 1400 m from the northwest model boundary, and between 1600 and 1800 m from the northwest model boundary in the low-lying areas corresponding to the different land surface profiles.

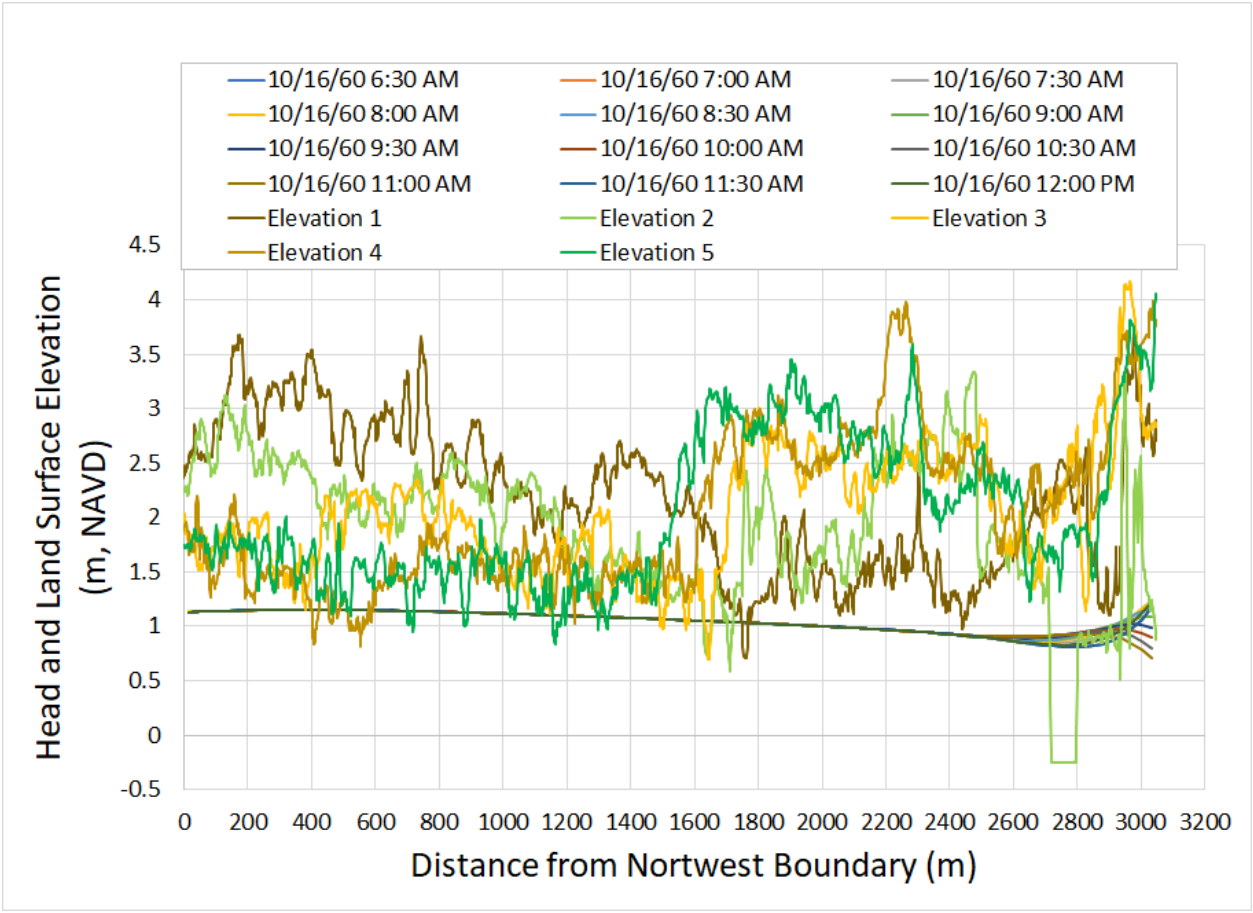

Figure 23. Land surface profiles Elevation 1 through Elevation 5 corresponding to the northeast to southwest series of traverses in Figure 22 and groundwater profile for a tidal cycle in 2060. Flooding occurs where the land surface drops below the water table.

6 Discussion

6.1 Potential impact of sea level rise and increased precipitation on flooding frequency

Comparing Figures 19 and 21, there are no historical 2016 groundwater levels above 0.9 m while under the 2060 scenario conditions there are clearly many days (34% of the year) when the projected groundwater elevation exceeds 0.9 m and flooding would be expected.

The use of the 2016 rainfall data in the 2060 projection leads to a situation in which there are no groundwater levels higher than the 1.5 m threshold for widespread flooding. This is due to the lack of more extreme precipitation events in 2016, the relatively small inland impact of tidal fluctuations even with 0.61 m of sea level rise, and the fact that a 0.61 m sea level rise elevates the average groundwater level by a similar amount, which leads to many exceedances of the 0.9 m threshold but not the 1.5 m threshold. Future work should probably consider a broader

range of rainfall/recharge scenarios that could enable more complete statistical characterization of future groundwater conditions.

The scenario approach to future precipitation projections outlined above has been used in a variety of studies over Florida (e.g. Aumen et al. 2015), and as stated, future precipitation is approximated by increasing 2016 precipitation by 10% at each time-step. An alternative approach to using the 10% precipitation increase is to directly utilize climate model output, such as the data included in the Coupled Model Intercomparison Project version 5 (CMIP5, Taylor et al. 2011), which could have potential for use as an estimated precipitation input for the 2060 model projections. However, the groundwater model has high spatial and temporal constraints for rainfall, namely ½ hourly rainfall on a 2km x 2km grid. Spatially, climate models included in CMIP5 have resolutions that range from around 0.5 degrees latitude x 0.5 degrees longitude to 4 degrees latitude by 4 degrees longitude, and temporally from 3 hourly to monthly (Taylor et al. 2011), which is too coarse for the groundwater model. While downscaled data exist to bring the CMIP5 data to finer spatial scales, (Maurer et al. 2007; Giorgi et al. 2009; Ning et al. 2011, 2012; Stefanova et al. 2012; Brekke et al. 2013, among many others), these data are often unavailable on the fine temporal scale necessitated by the groundwater model. This highlights the growing demand for predictions and projections on a broad range of spatial and temporal resolutions, for example through downscaling or increasing native climate model resolution (e.g. Kirtman et al., 2012).

6.2 Groundwater Model Parameter Estimates

The non-unique nature of the individual T (K) and S aquifer parameter estimates (Table 3) might be improved by a more sophisticated treatment of recharge that would attempt to independently estimate its value. However, many uncertainties about this most-difficult to estimate aspect of the model, such as its spatial distribution due to surfaces of varying permeability, variations in soil type, and the spatial distribution and effectiveness of different plants at removing water, would remain.

The estimated hydraulic conductivity of the aquifer with 75% of rainfall as recharge is 6.67×10^{-3} m/s (Table 3). The model aquifer was assumed to be uniformly 30.48 m thick so that its transmissivity is 0.2 m^2/s. Geostatistical interpolation of aquifer test data by Hughes and White (2016, Figure 16) suggested a transmissivity between 0.1 and 0.25 m^2/s in the Arch Creek area in close agreement with our estimate, while calibration of their county-wide Urban Miami-Dade model (Hughes and White, 2016, Figure 40) led to considerably higher values between 0.5 and 5 m^2/s. Our result is somewhat lower than previously published estimates for the aquifer in that area (0.3 to 1 m^2/s; Renken et al., 2005), but may be consistent with the anomalously low hydraulic conductivity of the upper Biscayne Aquifer noted by Fish and Stewart (1991) at well G-3300 and shown in Figure 4. Incorporation of more realistic subsurface geology into the model might result in different estimates of the transmissivity.

6.3 Upstream Boundary Conditions

Spur Canal No. 4 (Figure 2) might be an appropriate upstream boundary for more detailed modeling of the Arch Creek area, but time-variant stage data for that reach of the canal do not appear to be available. Given the Arch Creek area's status as Miami-Dade County's first Adaptation Action Area, its bellwether circumstances for the region and other coastal regions, and the likelihood of substantial investments in adaptation, redevelopment, and protection, additional dedication of resources towards monitoring seems appropriate.

Well G-3978 is a new 82.3-m deep well also located near the west end of our cross-sectional model that could prove useful in future analyses of groundwater in the Arch Creek area. It has just a handful of quarterly measurements so far (Table 6).

Table 6. Head data from well G-3978.

Date	Head (m, NAVD)
07/14/2016	0.0951
10/14/2016	0.235
01/10/2017	0.202
04/10/2017	0.153

These values are lower that the boundary values we selected, but may reflect downward gradients due to regional pumping. There are pumping centers throughout the region that generally exploit the lower portion of the Biscayne Aquifer. The pumping center nearest the study area is approximately 16 km to the southwest and is visible as a cone of depression on Figure 5. Its wells draw water from approximately 25-35 meters below the surface.

6.4 Seawater Intrusion and Variable Density Effects

Although the Biscayne Aquifer beneath the model area is indicated as having been intruded by saltwater since before 1995 (Prinos et al, 2014), we do not take any variable density impacts into account in our modeling thus far. The data that the saltwater intrusion line is based on are sparse when viewed in the context of our small model area and show diverging trends. USGS well G -3948S, which is approximately 1600 m north of the middle of our cross-section model, is 37 m deep and shows rising salinity, with chloride concentrations approaching and/or exceeding the 250 mg/L standard. Another well, G-894, is 23.2 m deep and located about 2000 m south of the western end of our model and has shown a large decrease in chloride concentrations from 3000 mg/L in the 1960s to less than 20 mg/L now. Well G-3978 near the west end of our cross-sectional model has just quarterly measurements so far and a chloride concentration of about 60 mg/L. Given the sparsity of these data and the quality of the calibration and validation

simulations, we are satisfied that salinity and variable density effects are unlikely to have major impacts on our current model.

6.5 Temperature Increases and Effect on Evapotranspiration

Our simplified approach to recharge does not account for the impact of very likely temperature increases leading to increases in evapotranspiration. This could reduce the overall amount of recharge and would probably affect its timing. The net effect would likely be some reduction in groundwater levels, but given the rapid response of the water table to precipitation events, the overall effect is not expected to be significant. Moreover, this approximation is consistent with an approach that intends to conservatively overestimate impacts by using the high sea level curve and the +10% precipitation.

6.6 Influence of Local Stormwater Management

A complex stormwater management system called the Arch Creek Estates Phase I and II system has been constructed in the study area. Phase I is located between West Dixie Highway and NE 18 Ave, and Phase II is on West Dixie Highway and NE 12 Ave. The system includes a drainage network underlying part of the area. Figure 24 shows the construction plan for the system, which is interconnected to adjacent systems. Thirteen 61 m deep Class V stormwater drainage wells were constructed for disposal of a portion of the storm water collected by the system. The wells (7 in Phase I and 6 in Phase II) and their pumps AC 1 and AC 2 were constructed to improve flood protection in the Arch Creek basin and drain an area of 341550 m^2. In the Phase I area, there is a created wetland/storage basin (located west of the pump AC 1) for supplementary treatment prior to injection or discharge to the Arch Creek canal.

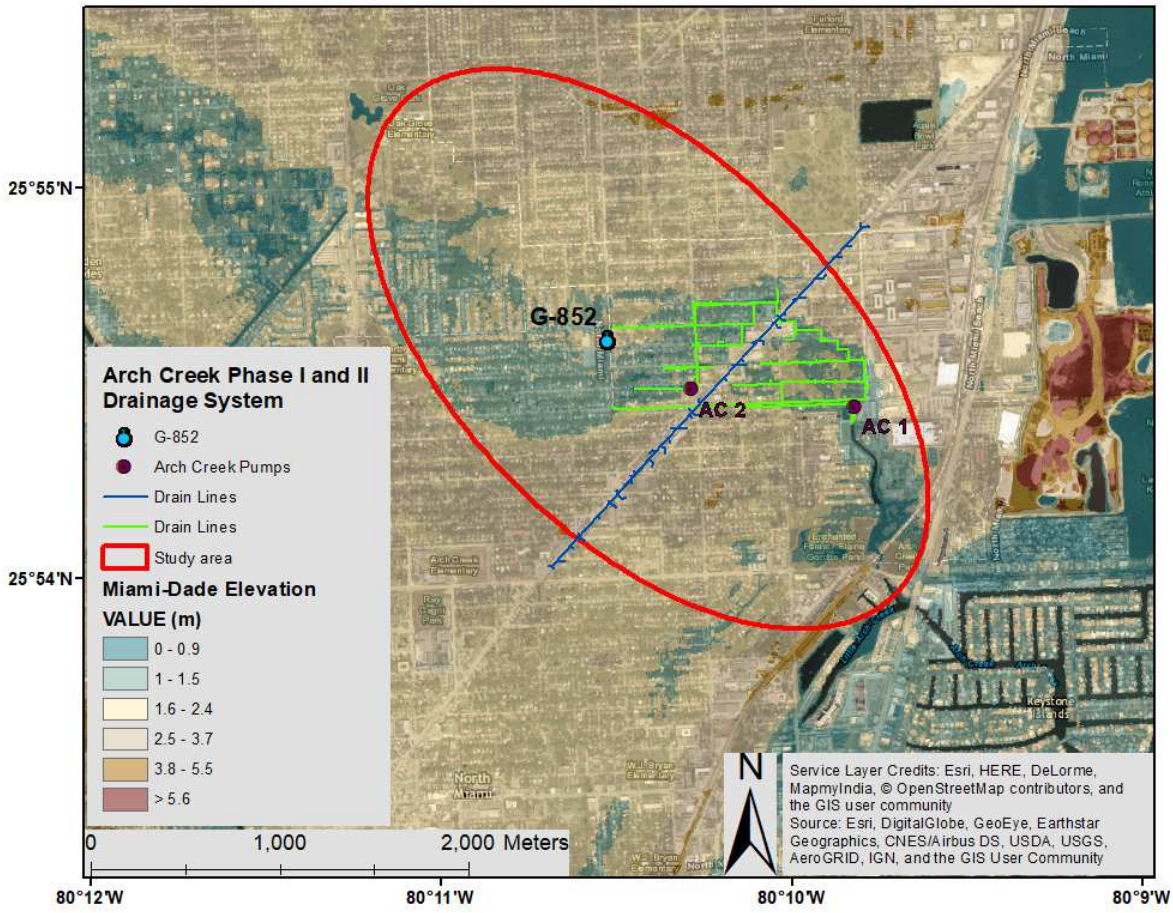

Figure 24. Arch Creek Estates Phase I and Phase II drainage network.

The significance of the operation of this system and its operation details are unknown and could not be obtained despite repeated requests, but could have an impact on groundwater conditions. Future modeling efforts might benefit from the permitting history of the system: the Miami-Dade Department of Environmental Resources Management (DERM) issued a final permit for the construction of the storm water drainage wells on June 13, 2002 and certification of the wells' construction completion on December 20, 2004. On July 20, 2006 a request for the modification of seven wells in Phase I was sent, and the construction permit was extended to June 12, 2007. Placing the wells into the service was authorized by DERM on November 21, 2008.

7 Conclusions

Areas in the Arch Creek basin that lie below 0.9 m NAVD elevation are particularly vulnerable to flooding and areas below 1.5 m NAVD are vulnerable to flooding from exceptionally large rainfall events. Groundwater modeling suggests that rain-induced short-term water table rises are a primary driver of flooding events under current conditions.

Analysis of long-term groundwater data indicates that the water table is rising at approximately the rate of local sea level. Linear extrapolation of long-term observed groundwater levels to 2060 suggest roughly a doubling of the number of historical days when groundwater levels exceed 0.9 m NAVD (from 93 days in the 43-year period from 6/27/1974 - 6/26/2017 to 177 days during the extrapolated period of 6/27/2017 - 6/26/2060) and a threefold increase in the number of days (from 3 to 9) when levels exceed 1.5 m NAVD. Because it is a linear extrapolation as opposed to the widely anticipated quadratic increase in sea level and involves no changes in precipitation, these estimates may conservatively underestimate future flooding.

Projected sea level rise of 0.61 m by 2060 together with 10% increased 2016 rainfall lead to a groundwater model prediction of frequent groundwater-related flooding in areas less than 0.9 m NAVD. However, current simulations do not consider the range of rainfall events that have led to water table elevations greater than 1.5 m NAVD and widespread flooding of the area in the past. A broader range of rainfall events need to be incorporated into the simulations to capture the statistical likelihood of these large-impact events under future sea level rise conditions.

Tidal fluctuations in the water table are predicted to be more pronounced within 600 m of the tidally influenced water control structure stage that is hydrodynamically connected to Biscayne Bay. The inland influence of tidal fluctuations appears to increase with increased sea level, but the principal driver of high groundwater levels under the 2060 scenario conditions remains groundwater recharge due to rainfall events.

The results provide a detailed look at a sea-level-rise-bellwether area and have physical, social, and policy relevance in the many similar areas that that experience flooding and will be subjected to sea level rise in the future.

Acknowledgements

This material is based on work supported by the National Science Foundation under Grant No. EAR-1204752. This is SERC contribution #___. We thank Daniel Gann of the Geographic Information Systems Center (GIS Center) at Florida International University for providing the Lidar data.

References

Aumen N.G., Havens K.E., Best G.R., Berry L. (2015) Predicting Ecological Responses of the Florida Everglades to Possible Future Climate Scenarios: Introduction. Environ Manage 55:741–748. https://doi.org/10.1007/s00267-014-0439-z

Banta, E.R., (2011), ModelMate—A graphical user interface for model analysis: U.S. Geological Survey Techniques and Methods 6–E4, 31 p. https://pubs.usgs.gov/tm/tm6e4/

Brekke L., Thrasher B., Maurer E., Pruitt T. (2013) Downscaled CMIP3 and CMIP5 climate projections: release of downscaled CMIP5 climate projections, comparison with preceding information, and summary of user needs.

Corum, J., 2016, A Sharp Increase In 'Sunny Day' Flooding, September 3, 2016, https://www.nytimes.com/interactive/2016/09/04/science/global-warming-increases-nuisance-flooding.html

Czajkowski, J., Engel, V.E., Martinez, C., Watkins, D., Hughes, J.D., and Sukop, M.C. (2018, this issue), Economic impacts of urban flooding in south Florida: Potential consequences of managing groundwater to prevent salt water intrusion, Science of the total Environment ___

Fish, J.E., and Stewart, M.T., 1991, Hydrogeology of the surficial aquifer system, Dade County, Florida: U.S. Geological Survey Water-Resources Investigations Report 90-4108, 50 p. https://sofia.usgs.gov/publications/wri/90-4108/wri904108.pdf

Franklin, J. L. and Brown, D.P. (2000), Tropical Cyclone Report Tropical Storm Leslie (Subtropical Depression One) 4-7 October 2000, National Hurricane Center, 5 November 2000, Revised 5 December 2000

Giorgi F, Jones C, Asrar GR (2009) Addressing climate information needs at the regional level: the CORDEX framework. World Meteorol Organ WMO Bull 58:175. doi: https://www.wmo.int/pages/publications/bulletin_en/archive/58_3_en/58_3_giorgi_en.html

Habel, S., C.H. Fletcher, K. Rotzoll, A.I. El-Kadi, 2017. Development of a model to simulate groundwater inundation induced by sea-level rise and high tides in Honolulu, Hawaii. Water Research, 114: 122 https://doi.org/10.1016/j.watres.2017.02.035

Hoover, D.J., K.O. Odigie, P.W .Swarzenski, and P.L. Barnard, 2016. Sea level rise and coastal groundwater inundation and shoaling at select sites in California. Journal of Hydrology: Regional Studies, 16 pp., http://dx.doi.org/10.1016/j.ejrh.2015.12.055

Hughes, J.D., and White, J.T., 2016, Hydrologic conditions in urban Miami-Dade County, Florida, and the effect of groundwater pumpage and increased sea level on canal leakage and regional groundwater flow (ver. 1.2, July 2016): U.S. Geological Survey Scientific Investigations Report 2014–5162, 175 p., http://dx.doi.org/10.3133/sir20145162.

Jacob, C.E., 1950, Flow of ground water, chapter 5, in Engineering Hydraulics: edited by H. Rouse, John Wiley, p. 321-386.

Kirtman B, Bitz C, Bryan F, et al (2012) Impact of ocean model resolution on CCSM climate simulations. Clim Dyn 39:1303–1328. https://doi.org/10.1007/s00382-012-1500-3

Markowitz A. and Stein, G. (1984), Chaos Reigns in Soggy Dade, Rain Tops 13 Inches on Beach, The Miami Herald, May 30, 1984, Page 1A

Maurer EP, Brekke L, Pruitt T, Duffy PB (2007) Fine-resolution climate projections enhance regional climate change impact studies. Eos Trans Am Geophys Union 88:504–504. https://doi.org/10.1029/2007EO470006

Miami-Dade, 2016, ARCH CREEK STUDY AREA, Miami-Dade County, Florida; Briefing Book for ULI Advisory Services Panel, May 22-27 2016 http://www.miamidade.gov/green/library/arch-creek-briefing-book.pdf

Miami-Dade, 2017, Repetitive losses, accessed June 26, 2017 http://www.miamidade.gov/environment/repetitive-losses.asp

Ning L., Mann M.E., Crane R., Wagener T. (2011) Probabilistic Projections of Climate Change for the Mid-Atlantic Region of the United States: Validation of Precipitation Downscaling during the Historical Era. J Clim 25:509–526. https://doi.org/10.1175/2011JCLI4091.1

Ning L., Mann M.E., Crane R., et al (2012) Probabilistic Projections of Anthropogenic Climate Change Impacts on Precipitation for the Mid-Atlantic Region of the United States. J Clim 25:5273–5291. https://doi.org/10.1175/JCLI-D-11-00565.1

NOAA (2017) Mean Sea Level Trend 8724580 Key West, Florida, https://tidesandcurrents.noaa.gov/sltrends/sltrends_station.shtml?stnid=8724580, Accessed August 28, 2017

Obeysekera, J., Barnes, J. and Nungesser, M. Climate Sensitivity Runs and Regional Hydrologic Modeling for Predicting the Response of the Greater Florida Everglades Ecosystem to Climate Change, Environmental Management (2015) 55: 749. https://doi.org/10.1007/s00267-014-0315-x

Pathak, C., 2004, Rainfall Estimates Using NexRad Technology, March 16, 2004 http://www.ce.utexas.edu/prof/maidment/GradHydro2010/Visual/SFWMD_Nexrad.pdf

Poeter, E.P., M.C. Hill, D. Lu, C. R. Tiedeman, and S. Mehl, 2014, UCODE_2014, with new capabilities to define parameters unique to predictions, calculate weights using simulated values, estimate parameters with SVD, evaluate uncertainty with MCMC, and More: Integrated Groundwater Modeling Center Report Number: GWMI 2014-02. http://igwmc.mines.edu/freeware/ucode/UCODE_2014_User_Manual-version02.pdf

Prinos, S.T., and Dixon, J.F., 2016, Statistical analysis and mapping of water levels in the Biscayne aquifer, water conservation areas, and Everglades National Park, Miami-Dade County, Florida, 2000–2009: U.S. Geological Survey Scientific Investigations Report 2016–5005, 42 p., http://dx.doi.org/10.3133/sir20165005.

Prinos, S.T., Wacker, M.A., Cunningham, K.J., and Fitterman, D.V., 2014, Origins and delineation of saltwater intrusion in the Biscayne aquifer and changes in the distribution of saltwater in Miami-Dade County, Florida: U.S. Geological Survey Scientific Investigations Report 2014–5025, 101 p., http://dx.doi.org/10.3133/sir20145025.

Renken, R.A., Dixon, J., Koehmstedt, J., Lietz, A.C., Ishman, S., Marella, R.L., Telis, P., Rogers, J., and Memberg, S., 2005, Impact of Anthropogenic Development on Coastal Ground-Water Hydrology in Southeastern Florida, 1900-2000: Reston, Va., U.S. Geological Survey Circular 1275, 77 p. https://pubs.usgs.gov/circ/2005/circ1275/

Rotzoll, K. and Fletcher, C.H., 2013. Assessment of groundwater inundation as a consequence of sea-level rise. Nature Climate Change. Volume 3, p. 477-481. https://doi.org/10.1038/nclimate1725

SFWMD, 2016, Historic 2015-2016 Dry Season Rainfall, Just the Facts Fact Sheet, February 2016, https://www.sfwmd.gov/sites/default/files/documents/jtf_2015-16_dry_season_rainfall.pdf

Stefanova L, Misra V, Chan S, et al (2012) A proxy for high-resolution regional reanalysis for the southeast United States: assessment of precipitation variability in dynamically downscaled reanalyses. Clim Dyn 38:2449–2466. https://doi.org/10.1007/s00382-011-1230-y

Sukop, M.C., and Cunningham, K.J. (2014), Lattice Boltzmann methods applied to large-scale three dimensional virtual cores constructed from digital optical borehole images of the karst carbonate Biscayne aquifer in southeastern Florida, Water Resour. Res., 50, http://dx.doi.org/10.1002/2014WR015465.

Taylor KE, Stouffer RJ, Meehl GA (2011) An Overview of CMIP5 and the Experiment Design. Bulletin of the American Meteorological Society 93:485–498. https://doi.org/10.1175/bams-d-11-00094.1

ULI (2016), Arch Creek Basin, Miami-Dade County, Florida, Addressing Climate Vulnerabilities and Social Equity with an Adaptation Action Area Framework, May 22–27, 2016; A ULI Advisory Services Panel Report, Urban Land Institute, Washington, DC, http://uli.org/wp-content/uploads/ULI-Documents/Miami_PanelReport.pdf

U.S. Army Corps of Engineers (1958), Draft Survey-Review Report on Central and Southern Florida Project, Arch Creek Area, June 13, 1958

U.S. Army Corps of Engineers (2015), Interim Approved Jurisdictional Determination Form, http://www.saj.usace.army.mil/Portals/44/docs/regulatory/JDs/Florida/CWR/20151005-CWR-SAJ-2013-00380-AJD-AWP.pdf

Wdowinski, S., R. Bray, B. P. Kirtman, and Z. Wu, 2016, Increasing flooding hazard in coastal communities due to rising sea level: Case study of Miami Beach, Florida, Ocean & Coastal Management, 126:1-8, http://dx.doi.org/10.1016/j.ocecoaman.2016.03.002

Winston, R.B., 2009, ModelMuse—A graphical user interface for MODFLOW–2005 and PHAST: U.S. Geological Survey Techniques and Methods 6–A29, 52 p., available only online at http://pubs.usgs.gov/tm/tm6A29.

Projected Intersection of Water Table with Land Surface at 2060 King Tide assuming 2016 Precipitation +10%